Cellular Microbiology (2015) **17**(3), 369–388

doi:10.1111/cmi.12373
First published online 31 October 2014

Epsilon toxin from *Clostridium perfringens* acts on oligodendrocytes without forming pores, and causes demyelination

Laetitia Wioland,[1] Jean-Luc Dupont,[1] Frédéric Doussau,[1] Stéphane Gaillard,[1] Flavia Heid,[1] Philippe Isope,[1] Serge Pauillac,[2] Michel R. Popoff,[2] Jean-Louis Bossu[1] and Bernard Poulain[1]*

[1]*Centre National de la Recherche Scientifique Associé à l'Université de Strasbourg, Institut des Neurosciences Cellulaires et Intégratives UPR3212, 5 rue Blaise Pascal, Strasbourg cedex F-67084, France.*

[2]*Institut Pasteur, Bactéries Anaérobies et Toxines, 25 rue du Dr Roux, Paris cedex15, F-75724, France.*

Summary

Epsilon toxin (ET) is produced by *Clostridium perfringens* types B and D and causes severe neurological disorders in animals. ET has been observed binding to white matter, suggesting that it may target oligodendrocytes. In primary cultures containing oligodendrocytes and astrocytes, we found that ET (10^{-9} M and 10^{-7} M) binds to oligodendrocytes, but not to astrocytes. ET induces an increase in extracellular glutamate, and produces oscillations of intracellular Ca^{2+} concentration in oligodendrocytes. These effects occurred without any change in the transmembrane resistance of oligodendrocytes, underlining that ET acts through a pore-independent mechanism. Pharmacological investigations revealed that the Ca^{2+} oscillations are caused by the ET-induced rise in extracellular glutamate concentration. Indeed, the blockade of metabotropic glutamate receptors type 1 (mGluR1) prevented ET-induced Ca^{2+} signals. Activation of the N-methyl-D-aspartate receptor (NMDA-R) is also involved, but to a lesser extent. Oligodendrocytes are responsible for myelinating neuronal axons. Using organotypic cultures of cerebellar slices, we found that ET induced the demyelination of Purkinje cell axons within 24 h. As this effect was suppressed by antagonizing mGluR1 and NMDA-R, demyelination is therefore caused by the initial ET-induced rise in extracellular glutamate concentration. This study reveals the novel possibility that ET can act on oligodendrocytes, thereby causing demyelination. Moreover, it suggests that for certain cell types such as oligodendrocytes, ET can act without forming pores, namely through the activation of an undefined receptor-mediated pathway.

Received 28 January, 2014; revised 29 August, 2014; accepted 29 September, 2014. *For correspondence. E-mail poulain@inci-cnrs.unistra.fr. Tel. (+33) 3 88 77 84 21; Fax (+33) 3 88 60 16 64

Introduction

The proliferation of *Clostridium perfringens* types B and D in the gut often causes lethal enterotoxaemia in sheep, goats and other ruminants, and the main aetiologic factor of the disease is epsilon toxin (ET), a ~ 30 kD peptide (reviewed in McClane *et al.*, 2006; Uzal and Songer, 2008; Bokori-Brown *et al.*, 2011; Popoff, 2011). The high lethality of ET (~ 400,000 mouse lethal doses per mg protein, intra-peritoneal) ranks this toxin among the four most potent poisonous substances known so far (reviewed in Gill, 1982).

To date, very little information is available about the mechanisms involved in ET-induced intoxicated host death during the naturally occurring disease. ET produced in the intestinal lumen crosses the intestinal mucosal barrier and disseminates throughout all organs via the blood flow. Consistent with the severe neurological disorders displayed during ruminant enterotoxaemia (reviewed in Wioland *et al.*, 2013), ET accumulates preferentially in the brain and kidneys (Nagahama and Sakurai, 1991). In rodents, ET binds to the luminal surface of the vascular endothelium (Soler-Jover *et al.*, 2007) and alters the blood–brain barrier (Zhu *et al.*, 2001; Soler-Jover *et al.*, 2007), favouring the formation of perivascular oedemas and toxin diffusion into neural tissue. The nervous tissue lesions are located in the cerebellum, and certain defined cerebral regions, and overall, the cerebellum is a site of predilection for the induction of early central nervous system alterations (reviewed in Finnie, 2004; Wioland *et al.*, 2013).

Growing evidence indicates that the numerous neurological disorders caused by ET result from neural tissue damages caused by the formation of brain oedemas

© 2014 The Authors. Cellular Microbiology published by John Wiley & Sons Ltd.
This is an open access article under the terms of the Creative Commons Attribution-NonCommercial-NoDerivs License, which permits use and distribution in any medium, provided the original work is properly cited, the use is non-commercial and no modifications or adaptations are made.

(Buxton and Morgan, 1976; Uzal and Kelly, 1997; Uzal *et al*., 1997) and/or the direct attack of some types of neural cells by ET. Indeed, we have shown in earlier studies that ET induces many effects in certain mouse neuron types such as cerebellar granule cells, but does not affect the glial cells of the astrocyte lineage (Lonchamp *et al*., 2010; Wioland *et al*., 2013). Several observations support the hypothesis that oligodendrocytes, whose protusions form the myelin sheath around the axons in white matter, are potential major targets for ET. Indeed, the central nervous system white matter is the prominent tissue component labelled by green fluorescent protein (GFP)-tagged ET in several species such as sheep, cattle, mice and humans (Dorca-Arévalo *et al*., 2008), and it is altered in infected animals (Buxton and Morgan, 1976; Finnie, 1984a,b; Uzal and Kelly, 1997; Uzal *et al*., 1997). Studies by Soler-Jover *et al*. (2007); Dorca-Arévalo *et al*. (2008) and Lonchamp *et al*. (2010) have found that ET co-localizes with myelin markers like myelin basic protein (MBP) or 2′,3′-cyclic nucleotide 3′-phosphodiesterase, both of which are proteins specifically expressed by oligodendrocytes. However, whether the oligodendrocytes and white matter are directly affected by ET remains to be established.

The cytotoxic effects of ET are believed to result from the initial formation of transmembrane pores (reviewed in Bokori-Brown *et al*., 2011; Popoff, 2011). The three-dimensional structure of ET displays many similarities with the pore-forming toxin aerolysin produced by *Aeromonas hydrophila* (Cole *et al*., 2004). It is currently suggested that seven ET monomers assemble on the membrane surface to create a pre-pore complex that inserts into the lipid bilayer, forming a transmembrane pore (Robertson *et al*., 2011). The conductance of ET pores is very high, ranging between 480 pS and 550 pS (Petit *et al*., 2001; Nestorovich *et al*., 2010). This pore-forming activity results in a dramatic decrease in the transmembrane electrical resistance produced by ET, as detected through the use of patch-clamp recordings in renal collecting duct mpkCCDcl4 murine cells (Chassin *et al*., 2007) and mouse cerebellar granule cells (Lonchamp *et al*., 2010). ET leads to multiple cell manifestations as such as glutamate efflux from mouse cerebellar granule cells (Lonchamp *et al*., 2010), higher intracellular Ca^{2+} concentration ($[Ca^{2+}]_i$), membrane swelling, loss of adenosine triphosphate (ATP), induction of oncosis and cell death (Petit *et al*., 1997; 2001; 2003; Chassin *et al*., 2007; Lonchamp *et al*., 2010). However, the relationship between these effects and ET pore-forming activity is not clear (Chassin *et al*., 2007; Lonchamp *et al*., 2010).

This study aimed to investigate the effects of ET on oligodendrocytes and myelin, *in vitro*. More specifically, we sought to determine whether ET binds to white matter in rat cerebellar slices and to oligodendrocytes in rat cerebellar cortex primary cultures, to ascertain whether this process induces glutamate efflux and intracellular oscillations in $[Ca^{2+}]_i$, and to establish whether it induces a loss of electrical resistance in the membrane, thus assessing the possibility of ET-forming pores in the latter. The use of organotypic cultures of rat cerebellar slices makes long-term *in vitro* exposure to ET possible, thus enabling us to also explore the possibility of this toxin-inducing myelin alteration.

Results

ET binds to white matter and oligodendrocytes in rat cerebellar slices

Acute cerebellar slices from (P25–P30) rats were incubated for 5 min with ET (10^{-7} M) before fixation and immunorevelation of bound ET. Figure 1A (green staining) shows no significant ET immunostaining in the molecular (Fig. 1Ai and Aii) and Purkinje cell layers [Fig. 1B; 28 kD protein (Calbindin) positive cells, red colour], with the exception of some capillary vessels. When similar experiments were performed without ET, a very low-intensity and non-specific signal was found on all cell types; this background signal is not illustrated. Prominent ET immunosignal was found both in the granular layer and in white matter. This rat white matter labelling is reminiscent of previous observations in the mouse cerebellum when ET (Lonchamp *et al*., 2010) or GFP-tagged ET (Dorca-Arévalo *et al*., 2008) was used. The marked ET-positive signal detected in the granular layer (Fig. 1B) was mostly located on fibre-like structures corresponding to myelinating protrusions of oligodendrocytes and myelinated axons. We observed a few cell somata decorated by intense ET labelling (indicated by arrow in Fig. 1B). These stained cells are too scarce to correspond to granule cells, the density of which exceeds 3.10^6 per mm^3 in the granular layer (Palay and Chan-Palay, 1974), and are probably oligodendrocyte somata and/or ET-stained protrusions of the perineuronal satellite oligodendrocytes that are wrapped around certain granule cell somata (Takasaki *et al*., 2010). Contrary to previous observations made using mouse cerebellum (Lonchamp *et al*., 2010; Wioland *et al*., 2013), no ET binding was immunorevealed on rat granule cells. The intense staining found in the cerebellar white matter is consistent with previous reports showing that the white matter in the central nervous system is the prominent component labelled by ET or GFP-tagged ET in several species (see Introduction). This, and the lack of detectable ET binding on granule cells, pinpoints the oligodendrocytes as the only major cell target in rat cerebellar tissue.

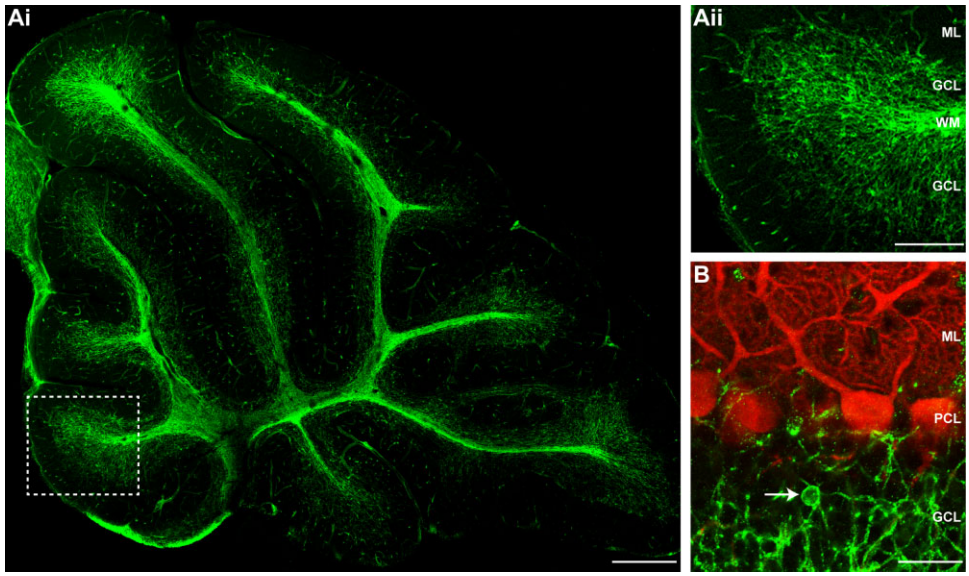


Fig. 1. ET binds to rat cerebellar white matter.
A. ET immunostaining (green) obtained when cerebellar slices were incubated with 10^{-7} M ET for 5 min before fixation. Ai. Whole rat cerebellum; scale bar = 500 μm. Aii. Magnification of region denoted by dotted frame in Ai, scale bar = 250 μm.
B. Cerebellar cortex was submitted to double immunostaining against ET (green) and the 28 kD protein (red), a Purkinje cell-specific marker. The arrow denotes an oligodendrocyte soma decorated by ET, scale bar = 50 μm. WM, white matter; GCL, granule cell layer; ML, molecular layer; PCL, Purkinje cell layer.

ET binds to oligodendrocytes, but does not bind to astrocytes in primary cultures of rat cerebellum

The ability of ET to bind to oligodendrocytes was examined on mixed primary cultures prepared from P0 to P1 rat cerebellum and grown for four days. Mature oligodendrocytes (as revealed by their positive immunoreactivity against MBP+ cells in Fig. 2) and astrocytes (positive immunoreactivity against glial fibrillary acidic protein, i.e. GFAP+ cells in Fig. 2) were the most abundant cells (64–72% and 18–30% of total number of cells respectively). Although oligodendrocytes cannot grow in the absence of astrocytes, the two cell types did not overlap each other in these cultures (Fig. 2Aiii) (Gaillard and Bossu, 1995; Boussouf *et al.*, 1997; Bernard *et al.*, 2001). Minor cell types were also present in the primary culture, of which 5–8% were microglial cells [positive immunoreactivity against ionized calcium binding adapter molecule 1 (Iba-1), data not shown] and 0.9–1.5% were granule cells (as revealed by their typical morphological shape and immunoreactivity against microtubule associated protein-2).

ET labelled most oligodendrocytes (MBP+ cells in Fig. 2B and C). When similar experiments were performed without ET, no cell was stained (not illustrated). Note the racket-shaped protrusions typical of mature-myelinating oligodendrocytes (Fig. 2Bii, Cii). As this labelling was obtained using low ET concentration (10^{-9} M), it is highly probable that oligodendrocytes express high-affinity ET receptor(s). However, ET did not bind to all oligodendrocytes (see Fig. 2D for an example of a MBP+/ET-negative oligodendrocyte). Indeed, the number of ET+ oligodendrocytes (i.e. significantly above the background signal) varied with the ET concentration used (Fig. 2E). Incubation with 10^{-9} M, 10^{-8} M, or 10^{-7} M ET yields 57.8%, 65.4% and 78.9% ET+ among the MBP+ cells respectively. These percentages were determined by analysing ET staining on 500 MBP+ cells from five cultures for the two lower toxin concentrations, and 1270 MBP+ cells from 10 distinct cultures for 10^{-7} M ET. This indicates that oligodendrocytes are heterogeneous in their ability to express ET receptors. We did not find any ET binding to MBP-negative bipolar cells, and consider that these cells are most probably the progenitor oligodendrocytes (data not shown).

Using 10^{-7} M ET for 5 min, no astrocytes (i.e. GFAP+ cells) displayed significant ET immunolabelling, as determined from 927 GFAP+ cells in five cultures (Fig. 2F). None of the microglial cells were stained by ET (data not shown). In complete contrast with findings in intact rat cerebellar slices (Fig. 1), the few contaminating granule cells were marked by ET 10^{-7} M, but not at lower concentrations (not illustrated). Following the application of 10^{-7} M ET for 5 min to rat cerebellar primary cultures that had been highly enriched in granule cells (prepared as described by Lonchamp *et al.*, 2010), all granule cells

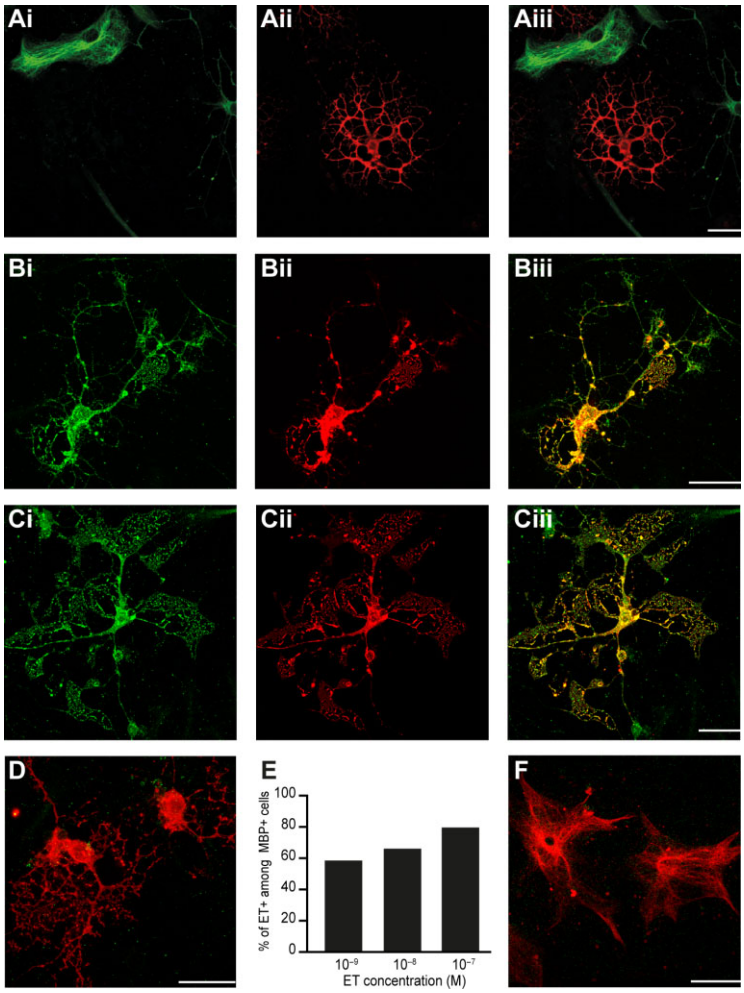


Fig. 2. ET binds to rat cerebellar oligodendrocytes in co-culture containing oligodendrocytes and astrocytes.
A. Rat cerebellar astrocytes and oligodendrocytes present in co-cultures were identified by their immunoreactivity to GFAP (green, Ai) or MBP (red, Aii) respectively. Aiii. Merge of GFAP and MBP immunoreactivities, scale bar = 50 μm.
B–D. ET immunostaining of oligodendrocytes obtained following application of ET (10^{-9} M, B; 10^{-7} M, C) for 5 min before fixation. Bi, Bii, Ci, and Cii. Immunostaining of ET (green) and MBP (red). Biii, Ciii. Their merged image. D. Same co-stainings, but showing an example of an oligodendrocyte that was not recognized by ET. A–C. Scale bars = 50 μm.
E. Bar chart reporting the fraction (%) of MBP+ cells (i.e. oligodendrocytes) labelled by ET following incubation with 10^{-9} M (% determined from $n = 500$ MBP+ cells in five different culture dishes), 10^{-8} M (% from $n = 500$ MBP+ cells in five different culture dishes), and 10^{-7} M (% from $n = 1270$ MBP+ cells in 10 different culture dishes) ET.
F. A typical example of lack of astrocyte staining by ET following incubation of the co-culture with the toxin (10^{-7} M) for 5 min before fixation. Merged image of ET (green) and GFAP (red) immunoreactivities. Scale bar = 50 μm.

were found to be ET+. These findings suggest that although ET does not recognize rat granule cells in intact neural tissue (Fig. 1), the latter still have the potential to express ET receptors.

ET induces an increase in the extracellular glutamate concentration by acting on oligodendrocytes

When injected intravenously or directly into the cerebral tissue, ET triggers glutamate efflux (Miyamoto *et al.*, 1998; 2000). As this amino acid is present at a millimolar concentration in the cytosolic compartment of all glial cell types (reviewed by Nedergaard *et al.*, 2002), extracellular glutamate can originate from any cell type, provided it is affected by ET. We examined the possibility that this toxin induces glutamate release from oligodendrocytes. Primary cultures were washed for 5 min with a physiological medium containing no glutamate, then treated with ET for 5 or 20 min (10^{-9} M: Fig. 3Ai; 10^{-7} M, Fig. 3Aii). Figure 3A shows that exposure to 10^{-9} M or 10^{-7} M of ET for 5 min induced a significant increase of up to ~1.5 10^{-6} M in the extracellular concentration of glutamate ($[glutamate]_e$), compared with the basal level values ('ctl' bars in Fig. 3) obtained in untreated cells. The $[glutamate]_e$ rise remained lower than that obtained by osmotic cell lysis ('lysis' bars, Fig. 3). No further significant increase was detected following incubation with ET for 20 min compared with the increase for 5 min incubation (Fig. 3A, compare 'ET5' and 'ET20' bars), suggesting that the rise in $[glutamate]_e$ reaches near completion in 5 min or less.

To verify that the rise in $[glutamate]_e$ was specifically due to ET and not to the presence of co-purified contaminants, we examined whether the change in $[glutamate]_e$ could be prevented by neutralizing ET with the very same specific anti-ET antibodies that we used for immunorevealing ET binding (neutralization assessment is described in the Material and Methods). No $[glutamate]_e$ rise occurred when 10^{-9} M ET was pre-incubated with antibodies at a 1 : 1 ratio for 20 min at room temperature

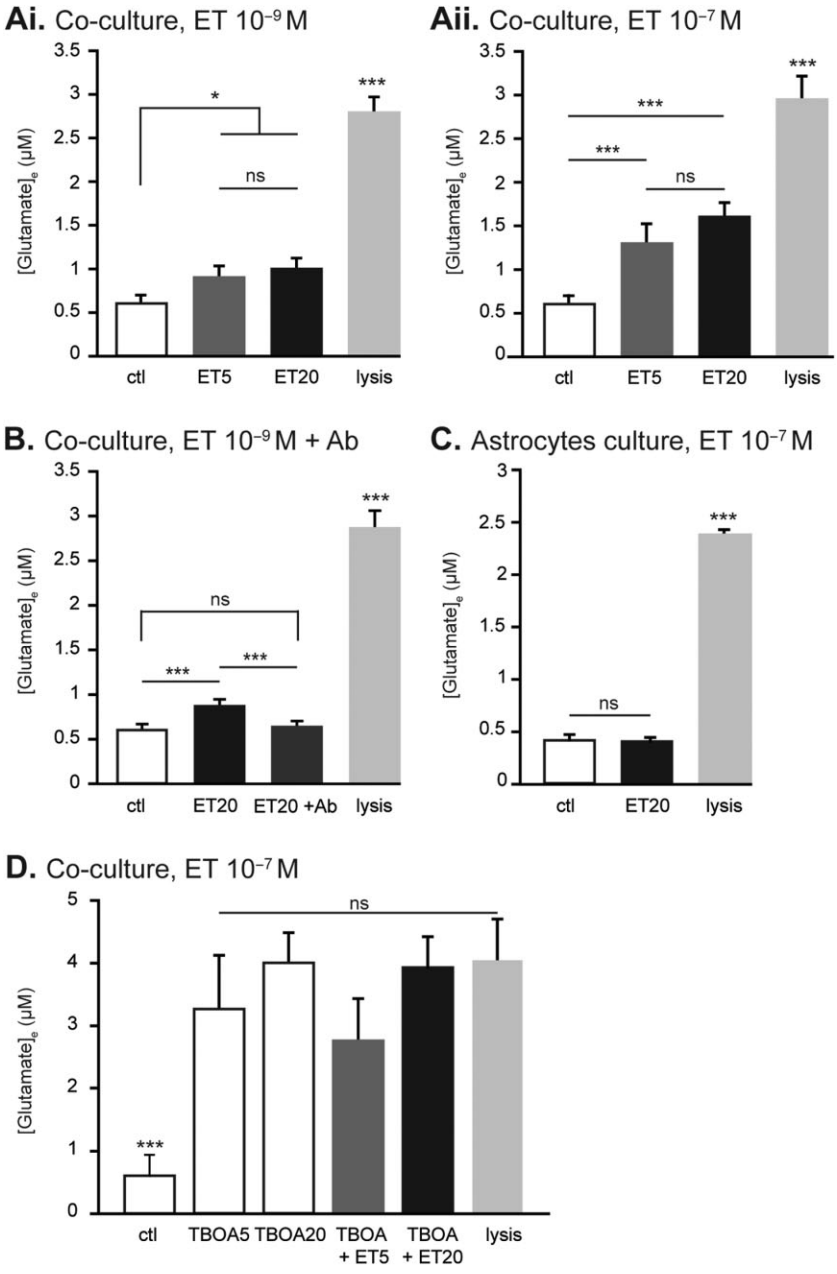


Fig. 3. ET induces increase in $[glutamate]_e$.
A. $[glutamate]_e$ (μM) determined in cultures containing oligodendrocytes and astrocytes (co-cultures) in the absence of ET (ctl, open bars), 5 min (dark grey bars) or 20 min (black bars) after ET application at 10^{-9} M (Ai) or 10^{-7} M (Aii), or after cell lysis (light grey bars) induced by hypo-osmotic shock.
B. The same after ET (10^{-9} M) application for 20 min, alone (black bar) or after preincubation with specific anti-ET antibodies (dark grey bars).
C. The same after ET (10^{-7} M) application to cultures containing astrocytes, but not oligodendrocytes.
D. $[glutamate]_e$ determined in control conditions (ctl), after 5 and 20 min in the presence of TBOA (10^{-4} M), with or without ET (10^{-7} M), or after cell lysis (light grey bars) induced by hypo-osmotic shock.
A–D. Means are from 27 determinations (triplicate measurements in nine independent experiments from three distinct cultures). Statistical significance: $^{*}P < 0.05$, $^{**}P < 0.01$, $^{***}P < 0.001$, ns. Stars on a bar in a chart denote that it differs from all the others.

(RT) before addition to the primary cultures (Fig. 3B). The $[glutamate]_e$ rise is therefore a specific effect induced by ET.

We next examined whether the ET effect on the oligodendrocytes is the primary cause of the observed $[glutamate]_e$ rise. To achieve this, primary cultures of rat cerebellum, which contained astrocytes, but no oligodendrocytes (see Material and Methods) were incubated with ET (10^{-7} M, for 20 min). No significant change was detected in $[glutamate]_e$ (Fig. 3C), indicating that the rise in $[glutamate]_e$ is primarily due to a specific effect of ET on oligodendrocytes. Cultured rat oligodendrocytes have a high uptake capacity and affinity for glutamate (DeSilva *et al.*, 2009). Like astrocytes, they are able to release glutamate in several circumstances, notably through glutamate transporter reversal (reviewed by Danbolt, 2001; Nedergaard *et al.*, 2002). We therefore investigated if the blockade of the plasma membrane glutamate transporters could interfere with ET action. DL-threo-beta-benzyloxyaspartate (TBOA) is a well-characterized potent blocker of all the glutamate transmembrane transporters expressed by glial cells (Shimamoto *et al.*, 1998; Domercq and Matute, 1999; Danbolt, 2001; Pitt *et al.*, 2003; DeSilva *et al.*, 2009). When TBOA (10^{-4} M) was applied to the

cultures, for either 5 or 20 min, $[glutamate]_e$ levels increased substantially (see the 'TBOA5' and 'TBOA20' bars in Fig. 3D) compared with control values ('ctl' in Fig. 3D). These data indicate that basal $[glutamate]_e$ is a dynamic equilibrium maintained at a low level through the uptake of glutamate by oligodendrocytes or/and astrocytes. When the experiments were repeated using a joint application of TBOA (10^{-4} M) and 10^{-7} M ET, for 5 or 20 min, $[glutamate]_e$ levels did not rise any higher than when TBOA was applied alone. These experiments suggest that the blockade of glutamate transporters prior to ET application interferes with the effect of ET on oligodendrocytes. Our data confirm the deduction mentioned earlier that ET-induced elevation of $[glutamate]_e$ results from a primary effect on oligodendrocytes. This does not however exclude the possibility that the increase in $[glutamate]_e$ could be amplified by a secondary indirect action on astrocytes, mediated by glutamate itself (i.e. a glutamate-induced glutamate release mechanism, Nedergaard *et al.*, 2002).

ET does not cause oligodendrocyte lysis or death, and does not form pores in their membrane

In addition to the change in glutamate membrane transport (addressed earlier), the oligodendrocyte-dependent, ET-induced increase in $[glutamate]_e$ may also result from oligodendrocyte lysis/death. Whether 10^{-7} M ET was applied for 5 or 20 min, no significant increase in the enzymatic activity of glucose-6-phosphate hydrogenase (a cytosolic enzyme) was detected in the extracellular medium. Note that high levels of this enzymatic activity were detected upon lysing the cells with osmotic shock (Fig. 4A). We did not find any evidence of ET-induced cell death. Indeed, following the incubation of culture containing oligodendrocytes with ET 10^{-7} M for durations of up to 24 h, the percentage of oligodendrocytes stained by trypan blue remained very low and unchanged in comparison with control experiments performed without ET (Fig. 4B). Note that after treatment with the fixative agent para-formaldehyde (PFA) (4% for 1 h), almost all the oligodendrocytes were stained by trypan blue. We can therefore state that the increase in $[glutamate]_e$ is not due to oligodendrocyte membrane lysis or to the death of these cells.

ET does not form pores in their membrane

In principle, the oligodendrocyte-dependent ET-induced increase in $[glutamate]_e$ could result from leakage of glutamate because of the formation of ET pores in the plasma membrane. Indeed, the small molecular weight of glutamate (~ 150 Da) is below the cut-off size (~ 2300 Da) determined for the intracellular side of ET pores (Nestorovich *et al.*, 2010). As we observed earlier (Chassin *et al.*, 2007; Lonchamp *et al.*, 2010), ET pores are manifested by a decrease in transmembrane electrical resistance (R_m), the extent of which is proportional to

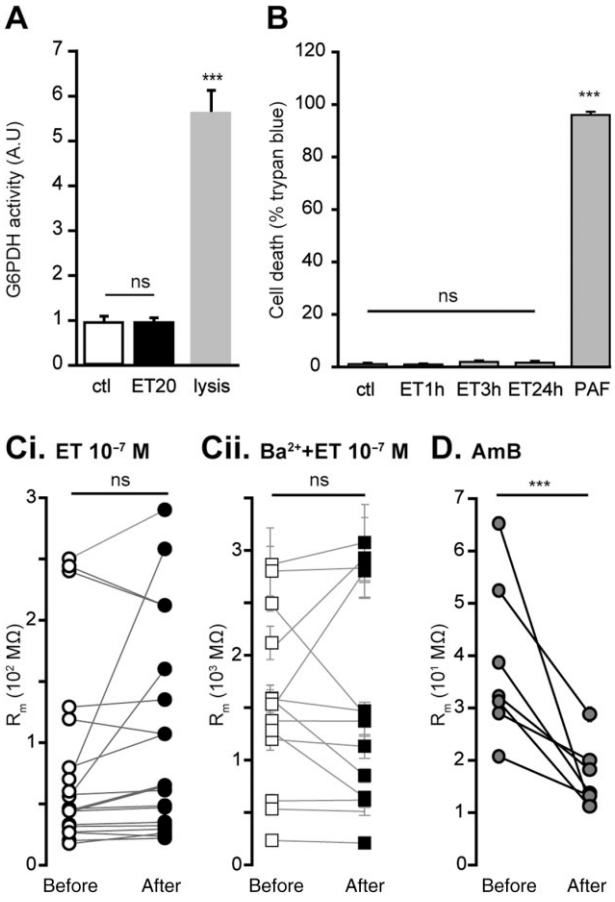


Fig. 4. ET does not induce membrane leakage, cell death or pore formation.
A. G6PDH activity determined in the absence of ET (ctl, open bar), 5 (dark grey bars) and 20 min (black bars) after ET 10^{-7} M application, or after cell lysis (light grey bars) induced by hypo-osmotic shock. Means are from 27 determinations (triplicate measurements in nine independent experiments from three distinct cultures).
B. Relative fraction of oligodendrocytes stained by trypan blue (i.e. dead cells) before (ctl), after ET 10^{-7} M application for 1, 3 or 24 h, or for 1 h after addition to the PFA fixative agent for 1h.% determined from 566, 474, 557,500 and 616 cells from five Petri dishes.
Ci. Average individual oligodendrocyte R_m determined before (open circles) and after (black circle) application of ET (10^{-7} M). Paired determinations, $n = 18$.
Cii. Same type of experiment, except that $BaCl_2$ (10^{-4} M) was present in the extracellular medium, before and after ET (10^{-7} M). Paired determinations $n = 14$. Note that because of the high increase in R_m following $BaCl_2$ applications, each data point presents a mean of four series of R_m determinations before and after ET was applied (i.e. 13.3 ± 1.1 min after ET).
D. Average individual oligodendrocyte R_m determined before and 10 min after AmB application (16.5 10^{-6} M final). Paired determinations, $n = 7$.
A–D. Statistical significance as in Figure 3.

the number of open pores. Using the patch-clamp technique, we performed individual cell measurements of R_m on mature oligodendrocytes (identified morphologically) before and after ET application. Prior to ET application, average oligodendrocyte Rm was 85.4 ± 18.7 MΩ ($n = 18$, from 18 Petri dishes). This R_m value is close to that previously determined with rat oligodendrocytes in acute slices (Gipson and Bordey, 2002). As ET leads to significant increases in $[glutamate]_e$ levels within 5 min or less (see earlier), R_m was determined in ET-treated oligodendrocytes after an average of 6.7 ± 0.7 min (same cells as in control). No significant change was found in Rm ($R_{m(ctl)} = 85.4 \pm 18.7$ and $R_{m(ET)} = 104 \pm 21$ MΩ, $n = 18$; paired *t*-test: $P = 0.75$; Fig. 4Ci), indicating that ET does not form pores in oligodendrocytes.

To exclude any possibility whatsoever of an ET pore forming in the oligodendrocyte plasma membrane, we performed additional experiments designed to increase R_m to such an extent that the formation of an ET pore could be detected by a marked decrease in R_m. Oligodendrocyte R_m is mostly determined by the presence of inwardly rectifying potassium channels (Kir channels, reviewed in Olsen and Sontheimer, 2008; Hibino *et al*., 2010), which are selectively blocked by Ba^{2+} ions (100 μM, Hagiwara *et al*., 1978; Gaillard and Bossu, 1995; Gipson and Bordey, 2002). The addition of 100 μM $BaCl_2$ prior to the application of 10^{-7} M ET to cultures caused a very marked (~ 20 fold) increase in oligodendrocyte R_m (compare data in Fig. 4Ci and Cii, drawn from different sets of experiments). When individual R_m determined for the 4 min preceding ET application was compared with individual R_m determined 13.3 ± 1.1 min after ET, no significant change was detected (average of pooled data: $R_{m(Ba^{2+})} = 1554 \pm 232$ MΩ, $Rm_{(Ba^{2+}+ET)} = 1527 \pm 287$, $n = 12$; paired *t*-test: $P = 0.88$, Fig. 4Cii), thereby confirming the findings mentioned earlier. We also checked that the presence of Ba^{2+} did not prevent ET binding to cultured oligodendrocytes (data not shown). In the presence of 10^{-4} M Ba^{2+}, the average resting membrane conductance ($G_m = 1/R_m$) of individual oligodendrocytes was ~ 650 pS, compared with ~ 10 000 pS without Ba^{2+}. Therefore, the opening of a single ET pore (~ 500 pS, Petit *et al*., 2001; Nestorovich *et al*., 2010) should have been shown by an increase in G_m to 1150 pS (i.e. 650 pS added to 500 pS) and a corresponding decrease in R_m by a factor of ~ 1.75. For each recorded cell, the careful examination of the individual plots of R_m (as determined every min) against time did not show any abrupt changes – even transitional – with a factor of 1.5–2.0 (not illustrated). In three out of 12 oligodendrocytes, a very slow decrease was observed in R_m (a kind of rundown, resulting in a lower R_m (by factor of ~ 2) within 10–12 min (Fig. 4Cii). However, the very slow kinetic of this decrease is inconsistent with that of an ET pore opening, which occurs within a few milliseconds. The absence of ET-induced changes in oligodendrocyte R_m (Fig. 4Ci and Cii) therefore rules out any possibility of ET causing any pore formation whatsoever in the oligodendrocytes. We then carried out an additional experiment to test whether an unrelated pore-forming agent could create pores in the oligodendrocyte plasma membrane. The pore-forming antibiotic amphotericin B (AmB, reviewed by Cohen, 2010) was indeed seen to affect R_m, with AmB ($16.5\ 10^{-6}$ M) inducing a rapid (in 2.5–6.0 min) and marked decrease in oligodendrocyte R_m (Fig. 4D).

ET induces intracellular [Ca^{2+}] oscillations in cultured oligodendrocytes

ET induces a $[Ca^{2+}]_i$ increase in both renal cell lines and cultured cerebellar granule cells (Chassin *et al*., 2007; Lonchamp *et al*., 2010), but the relationship between this increase and the pore-forming activity of the toxin remains to be established. To determine whether this ET effect occurs in oligodendrocytes, individual cellular cytoplasmic changes in $[Ca^{2+}]_i$ were monitored in morphologically mature oligodendrocytes (1 cell monitored per dish) pre-loaded with the Oregon Green 1,2-bis(o-aminophenoxy)ethane-N,N,N',N'-tetraacetic acid (BAPTA-1) acetyloxymethyl (AM) calcium probe. For each of the monitored cells, fluorescence intensity (F) was continuously recorded for at least 5 min before (F_0) and 30 min after ET application. No or very few spontaneous $[Ca^{2+}]_i$ oscillations were detected in untreated oligodendrocytes (Fig. 5Ai). However, many intracellular Ca^{2+} signals were induced following ET application (10^{-9} M in Fig. 5Aii; 10^{-7} M in Fig. 5Aiii). All changes in $[Ca^{2+}]_i$ were determined for each of the analysed cells (Table 1): mean $\Delta F/F_0$ (Fig. 5Bi), latency before the first Ca^{2+} signal (Fig. 5Bii), and cumulative duration during which $[Ca^{2+}]_i$ was above baseline values (Fig. 5Biii). Following ET application, average fluorescence intensity over 30 min became significantly higher ($P < 0.01$) than that determined for control experiments performed without ET (control: $\Delta F/F_{0(ctl)} = 0.008 \pm 0.006$, $n = 8$, individual values are in Fig. 5Bi, open circles; ET 10^{-7} M: $\Delta F/F_{0(ET)} = 0.205 \pm 0.037$, $n = 34$, see individual values in Fig. 5Bi, black circles; see also Table 1). We also noticed that a fraction (8 of 34; i.e. ~ 24%) of the recorded oligodendrocytes did not show any response to ET via significant change in $[Ca^{2+}]_i$ within the 40 min following ET application. As the proportion of responding oligodendrocytes (76%) is similar to that observed in ET-labelled oligodendrocytes (79%, see Fig. 2), the non-responding cells (~24%) may correspond to oligodendrocytes that do not express the ET receptor (~21%). In responding oligodendrocytes, the latency between ET application and the first $[Ca^{2+}]_i$ oscillation observed was on average 12.8 ± 1.8 min (Fig. 5Bii). The

© 2014 The Authors. Cellular Microbiology published by John Wiley & Sons Ltd,

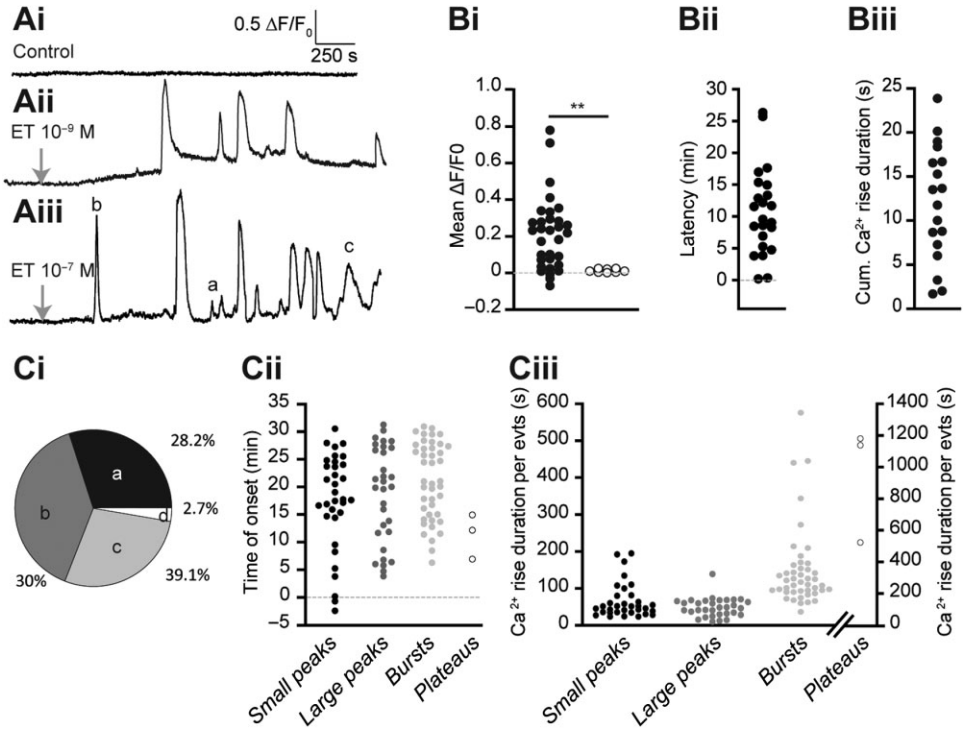


Fig. 5. ET induces intracellular $[Ca^{2+}]_i$ rise in oligodendrocytes. Changes in $[Ca^{2+}]_i$ were monitored by determining the relative changes in fluorescence ($\Delta F/F_0$) of cells loaded by the Oregon green probe.
A. Typical examples of $\Delta F/F_0$, plotted against time (min) in an oligodendrocyte in the absence (control) or after application (arrow) of ET (10^{-9} M, Aii; 10^{-7} M Aiii). Note the $[Ca^{2+}]_i$ oscillations appearing after ET application.
B. Quantification of the Ca^{2+} signals induced by ET. Each data point corresponds to the analysis of a cell recorded in one culture dish. Bi. Average $\Delta F/F_0$ determined over 30 min, in the absence of ET (control condition, open circles, $n = 8$) or starting after 10^{-7} M ET application (filled circles). $n = 34$, two asterisks denote $P < 0.01$. Note that 26 of the 34 cells did not respond to ET by a significant increase in $\Delta F/F_0$. Bii. Latency (min) before appearance of the first ET-induced Ca^{2+} signals (determined from the 23 responding cells). Biii. Cumulative time during which $\Delta F/F_0$ was over baseline values for the first 30 min after ET application (determined from 18 responding cells displaying no rundown of $\Delta F/F_0$ before ET application).
C. Characteristics of the individual ET-induced Ca^{2+} signals, sorted according to their kinetics and amplitude: peaks of small (a, black) or large (b, dark grey) amplitude, bursts of overlapping peaks (c, light grey), and plateau events (d, white). Ci. Pie chart representing their relative proportions (%). Cii. Their respective times of onset, and, Ciii, duration.

period of time during which $[Ca^{2+}]_i$ was higher than basal values varied significantly from cell to cell (Fig. 5Biii).

The ET-induced $[Ca^{2+}]_i$ oscillations were comprised of different types of Ca^{2+}-events (Fig. 5A), which could be sorted into four categories (see pie chart in Fig. 5Ci) including peaks of small (28%) or large (30%) amplitude, bursts of overlapping peaks (39%), and rare plateau events during which $[Ca^{2+}]_i$ levels remained high for minutes before subsiding (3%). By their time of onset (Fig. 5Cii) and duration (Fig. 5Ciii), the three former types of Ca^{2+} events (total = 97%) appeared to belong to the same class.

ET-induced [Ca^{2+}]$_i$ oscillations are due to the stimulation of metabotropic glutamate receptors

The short-living, ET-induced intracellular Ca^{2+} events described earlier are highly reminiscent of the $[Ca^{2+}]_i$ oscillations produced by neurotransmitter application to oligodendrocytes and/or Ca^{2+} release from intracellular Ca^{2+} stores in glial cells (Charles *et al.*, 1991; Cornell-Bell and Finkbeiner, 1991; Verkhratsky and Kettenmann, 1996; Butt, 2006; Luyt *et al.*, 2006; Nedergaard *et al.*, 2010). We examined whether the ET-induced $[Ca^{2+}]_i$ oscillations depended on the presence of extracellular Ca^{2+}. About 5 min prior to ET application, the control extracellular medium was replaced by a modified milieu containing 4 mM $MgCl_2$ and 0 mM $CaCl_2$. When ET 10^{-7} M was added, no Ca^{2+} event was observed and the average change in fluorescence was not distinct from control experiments performed without ET ($\Delta F/F_{0(ET\ 0\ Ca^{2+})} = 0.01 \pm 0.02$, ns, $n = 8$). As intracellular Ca^{2+} stores in many cell types can be quickly exhausted when extracellular Ca^{2+} is removed, we tested this possibility. In the absence of extracellular Ca^{2+}, 10 mM final application of caffeine (a drug that recruits

Table 1. Pharmacology of ET-induced Ca^{2+} signals.

Conditions	Control		Thapsigargin		Dantrolene		2-APB		D-APV		JNJ		Glut 10^{-5} M	Glut 10^{-6} M
ET	+	–	+	–	+	–	+	–	+	–	+	–		
$\Delta F/F_0$ (U.A)	0.2 ± 0.04	0.01 ± 0.01	0.03 ± 0.03	0.03 ± 0.01	0.15 ± 0.04	0.002 ± 0.004	0.03 ± 0.03	0.01 ± 0.01	0.08 ± 0.03	0.01 ± 0.01	0.01 ± 0.02	0.02 ± 0.01	0.45 ± 0.17	0.14 ± 0.06
Statistical significance	**		ns		**		ns		**		Ns			
Latency (min)	12.8 ± 1.76	–	–	–	6.56 ± 1.14	–	–	–	17.51 ± 0.8	–	–	–	14.82 ± 2.8	16.95 ± 1.2
Cum. Ca^{2+} rise duration (min)	12.02 ± 1.55	–	–	–	20.07 ± 1.91	–	–	–	5.34 ± 0.98	–	–	–	16.5 ± 2.12	5.08 ± 2.94
Cell number	34	8	12	7	12	7	10	7	14	8	10	7	6	5

2-APB, 2-aminoethoxydiphenyl borate; D-APV, 2R-amino-5-phosphonopentanoate; JNJ, $JNJ_{16259685}$. Two asterisks denote $P < 0.01$.

Ca^{2+} reticular stores by activating the ryanodin receptors, RyR) failed to induce any increase in $[Ca^{2+}]_i$ [$\Delta F/F_{0(Caffeine\ 0\ Ca2+)} = 0.01 \pm 0.01$, $n = 8$, not significant (ns)], whereas an increase was observed in the presence of extracellular Ca^{2+}-containing medium ($\Delta F/F_{0(Caffeine)} = 0.17 \pm 0.04$, $P < 0.001$, $n = 9$). The loss of ET effect in the absence of extracellular Ca^{2+} might therefore be due to the exhaustion of intracellular Ca^{2+} stores, and/or a lack of Ca^{2+} influx through channels conducting store-operated Ca^{2+} entry or ligand-gated channels, with the exception of the voltage-dependent Ca^{2+}-channels that are not expressed by mature oligodendrocytes (reviewed by Verkhratsky and Kettenmann, 1996; Butt, 2006; Nedergaard *et al.*, 2010). Thapsigargin (10^{-6} M) was applied to cultures for 30 min in order to exhaust endoplasmic reticulum (ER) Ca^{2+} stores by blocking the SERCA (Sarco/ER Ca^{2+} ATPase) pump. Following this pretreatment, which induced a moderate stable increase in basal $[Ca^{2+}]_i$ (data not shown), ET (10^{-7} M) did not induce Ca^{2+} signals (an example of 30 min continuous recording is provided in Fig. 6Ai). Data are summarized in Fig. 6Aiv, and Table 1. To determine whether the Ca^{2+} signals were induced by activation of the RyR and/or IP_3-receptors (IP_3-R), cultures were pretreated for 30 min with Dantrolene (10^{-5} M) a specific blocker of the various RyR subtypes, or 2-aminoethoxydiphenylborane (2-APB, 10^{-4} M), a pharmacological agent that inhibits the various IP_3-R subtypes, but also most of the channels mediating store-operated Ca^{2+} entry, such as TRP and Orai channels (reviewed by Harteneck and Gollasch, 2011). ET was unable to induce Ca^{2+} signals after pre-incubation of cultures with 2-APB (Fig. 6Aii and Aiv), while Ca^{2+} signals were detected after treatment with dantrolene (Fig. 6Aiii and Aiv). A summary of data is displayed in Table 1. As oligodendrocytes can express TRPC3 (Fusco *et al.*, 2004) and rare Orai channels (Verkhratsky and Parpura, 2014), ET-induced Ca^{2+}-signals may be due to the mobilization of Ca^{2+} from the ER (because of the activation of IP_3-R, but not RyR) and/or store-operated Ca^{2+} entry. Further pharmacological investigation, including the possible upstream activation of phospholipase C, which catalyses IP_3 production, was found to be impossible due to the deleterious effect of the necessary drugs on oligodendrocytes.

As ET-induced increase in $[glutamate]_e$ reaches near completion in ~ 5 min (Fig. 3), yet the ET-induced Ca^{2+} intracellular events occurred later (after a delay of ~ 13 min, Fig. 5), therefore we next investigated the possibility that the latter were a consequence of the former. Indeed, the activation of glutamate receptors is one of the main events inducing Ca^{2+} signalling in mature oligodendrocytes, in response to either the activation of Ca^{2+}-permeable glutamate receptors (such as the N-methyl-D-aspartate receptor, also known as NMDA-R,

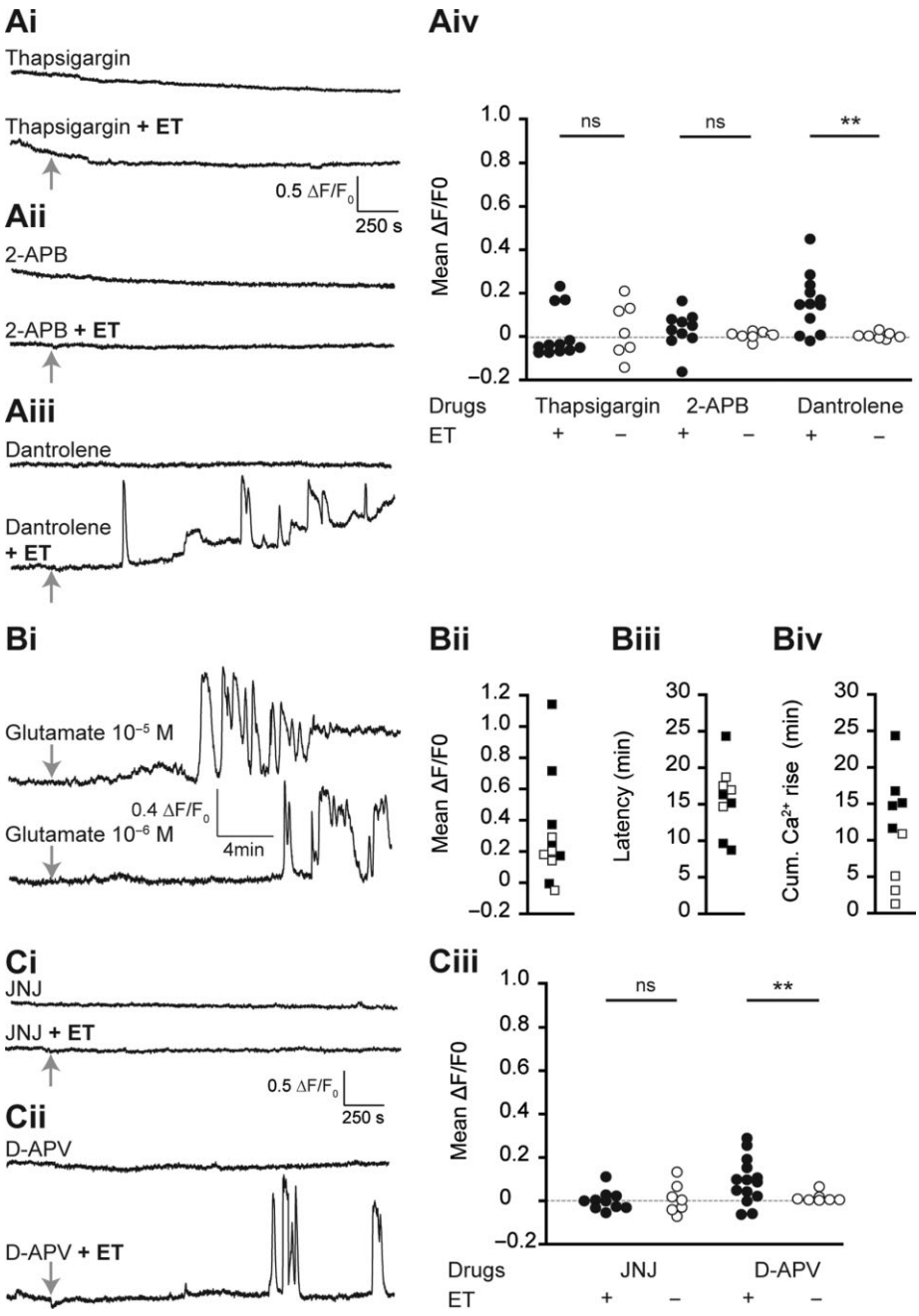


Fig. 6. Pharmacological dissection of ET-induced Ca^{2+} signalling pathway.
A. Typical examples of $\Delta F/F_0$ plotted against time in cultured oligodendrocytes in the presence of a pharmacological agent either alone (top recordings) or with ET (bottom recordings). The arrow denotes ET application time. Identical scale bars for all traces. Effects of treating cultures (in the absence or presence of 10^{-7} M ET) with: (Ai) the SERCA pump blocker thapsigargin (0.5 10^{-6} M), (Aii) the IP_3-R and store-operated Ca^{2+} entry antagonist 2-APB (10^{-4} M), or (Aiii) the RyR antagonist Dantrolene (10^{-5} M). Aiv. Summary of the pharmacological data. Mean $\Delta F/F_0$ determined over 30 min in the presence of the mentioned pharmacological agents, with (+) or without (–) of ET (10^{-7} M).
B. Glutamate-induced $[Ca^{2+}]_i$ rise in oligodendrocytes. Bi. Typical examples of changes in $\Delta F/F_0$ plotted against time and induced in oligodendrocytes by application of glutamate (10^{-5} M: top recording, or 10^{-6} M, bottom recording). Bii–Biv. Summary of the corresponding data (open squares: 10^{-6} M glutamate; filled squares: 10^{-5} M). Bii. Mean $\Delta F/F_0$ determined over 30 min in the presence of glutamate; Biii. Latency between glutamate application and first Ca^{2+} signal. Biv. Cumulative time during which $\Delta F/F_0$ was over baseline values, as determined over the first 30 min after glutamate application.
C. ET-induced $[Ca^{2+}]_i$ rise in oligodendrocytes was due to activation of glutamate metabotropic receptors. Ci. Typical changes in $\Delta F/F_0$ against time in cells pretreated with the mGluR1 specific antagonist $JNJ_{16259685}$ (2 10^{-6} M), with or without the presence of ET (10^{-7} M). Cii. Same type of experiment, with prior treatment of cells with NMDA–R-specific antagonist, D-APV (5 10^{-5} M). Scale bars identical to those in A. Ciii. Identical to Aiv.
A–C: $^{**}P < 0.01$, ns.

or the α-amino-3-hydroxy-5-methylisoxazole-4-propionic acid receptor, also termed AMPA-R) or the G-protein coupled glutamate metabotropic receptors (mGluR) from group I (mGluR1 and mGluR5), which activate phospholipase C and the ensuing production of IP_3 (reviewed in Butt, 2006). L-glutamate application to cultures (10^{-6} M or 10^{-5} M, Fig. 6B) induced Ca^{2+} signals in oligodendrocytes that were very similar to those induced by ET (Figs 5A and 6B). As the selective agonists of AMPA-R ((s)-AMPA) and mGlurR5 [(RS)-2-chloro-5-hydroxyphenylglycine] failed to induce Ca^{2+}-signalling (data not shown), it is likely that AMPA-R and mGluR5 are not expressed by oligodendrocytes under our culture conditions. These data are fully consistent with the down-regulation of AMPA-R (Alberdi *et al*., 2005; De Biase *et al*., 2010) and mGluR5 (Luyt *et al*., 2006) occurring when oligodendrocyte precursor cells differentiate into oligodendrocytes, in culture, and the progressive loss of Ca^{2+} oscillations induced by mGluR5 agonists (Luyt *et al*., 2006). Importantly, incubation with $JNJ_{16259685}$ (2 10^{-6} M), a highly potent and selective mGluR1 antagonist (Lavreysen *et al*., 2004), completely prevented the induction of Ca^{2+} events by ET 10^{-7} M (Fig. 6Ci and Ciii). While incubation with D-(-)-2-amino-5-phosphonovaleric acid (D-APV, 5 10^{-5} M), a specific blocker of NMDA-R, did not prevent the ET-induced Ca^{2+} oscillations (Fig. 6Cii and Ciii), it did cause a significant increased latency for the first ET-induced Ca^{2+}-signal (Table 1) and result in a lower cumulative Ca^{2+} rise (Table 1). Note that none of the drugs mentioned induced Ca^{2+} signals when used alone (see the control $\Delta F/F_0$ recordings in Fig. 6A and C). These results indicate that the activation of NMDA-R, which may mediate influx of Ca^{2+} from extracellular medium, is not responsible for the observed Ca^{2+} events induced by ET.

ET induces demyelination of Purkinje cells axons in the cerebellar granular layer

Oligodendrocytes are very sensitive to glutamate and Ca^{2+} signalling, which can lead to demyelination. Indeed, the binding of Ca^{2+} to calmodulin can not only cause the dissociation of MBP from actin and MBP from the membrane, but also dissociates the microtubules from MBP, thereby altering the myelin (reviewed in Harauz and Boggs, 2013). Excessive glutamate/Ca^{2+} signalling may also cause oligodendrocyte death and associated demyelination (reviewed in Matute *et al*., 2006; Bakiri *et al*., 2009; Matute, 2011). As ET induces $[glutamate]_e$ elevation and thus $[Ca^{2+}]_i$ oscillations, we investigated *in vitro* the possibility that ET may induce myelin alteration. To achieve this, organotypic cultures of P10–P11 rat cerebellar slices were prepared. After a 6-day period to allow myelination of Purkinje cells axons to develop *in vitro*, the slices were maintained for 24 h in a medium containing no toxin (control slices) or ET, then fixed. In the 'control' slices, numerous Purkinje cell (28 kD+ cells) axons crossing the granular layer were delineated by a MBP+ signal denoting the axons surrounded by myelin (Fig. 7A and B). When slices were incubated with ET (10^{-7} M), the MBP+ immunosignal was strongly diminished and the MBP+ structures were dramatically disorganized, while the 28 kD+ immunosignal and Purkinje cells structures remained similar to those observed in 'control' slices (Fig. 7C and D). Similar results, albeit less dramatic, were obtained using 10^{-9} M ET (data not shown). The effect of 10^{-7} M ET on myelination was quantified by counting MBP+ and 28 kD+ pixels from region of interest (ROI) selected from the upper region of the granular layer directly below the Purkinje cell layer (Fig. 7E). While the fraction (%) of 28 kD+ pixels in ROI was similar in the control condition and after ET (130 and 130 ROI analysed, P = ns; Fig. 7Ei), the fraction (%) of MBP+ pixels decreased dramatically after ET in comparison with control conditions ($P < 0.001$, Fig. 7Eii). Consistently, the fraction of MBP+ among 28 kD+ pixels also decreased significantly ($P < 0.001$, Fig. 7Eiii). These collective data indicate that ET induces marked demyelination of Purkinje cells axons, without damaging the Purkinje cells and their axons.

Demyelination is induced by an ET-induced rise in $[glutamate]_e$

To determine whether the ET-induced demyelination is causally linked to a $[glutamate]_e$ increase, as we observed in the primary cell cultures, the organotypic slices were incubated with ET (10^{-7} M) in the presence of $JNJ_{16259685}$ (2 10^{-6} M) and D-APV (5 10^{-5} M) to prevent the activation of both mGluR1 and NMDA-R respectively. Under this pharmacological condition, ET 10^{-7} M failed to induce significant demyelination (Fig. 8A and B). Note in Figure 8 the presence of numerous Purkinje cell axons in the granular cell layer (28 kD+) surrounded by myelin (MBP+) in the $JNJ_{16259685}$, D-APV, ET-treated slices. The result of the pixel analysis in ROI is presented in Fig. 8C. These data indicate that the demyelination caused by ET in cultured rat cerebellar slices is triggered by an initial $[glutamate]_e$ increase caused by ET.

Discussion

ET binds to myelin and oligodendrocytes and acts on them

The binding of ET to rat brain white matter and rat oligodendrocytes in primary culture is fully consistent with previous studies performed with other animal species (see Introduction, and Soler-Jover *et al*., 2007;

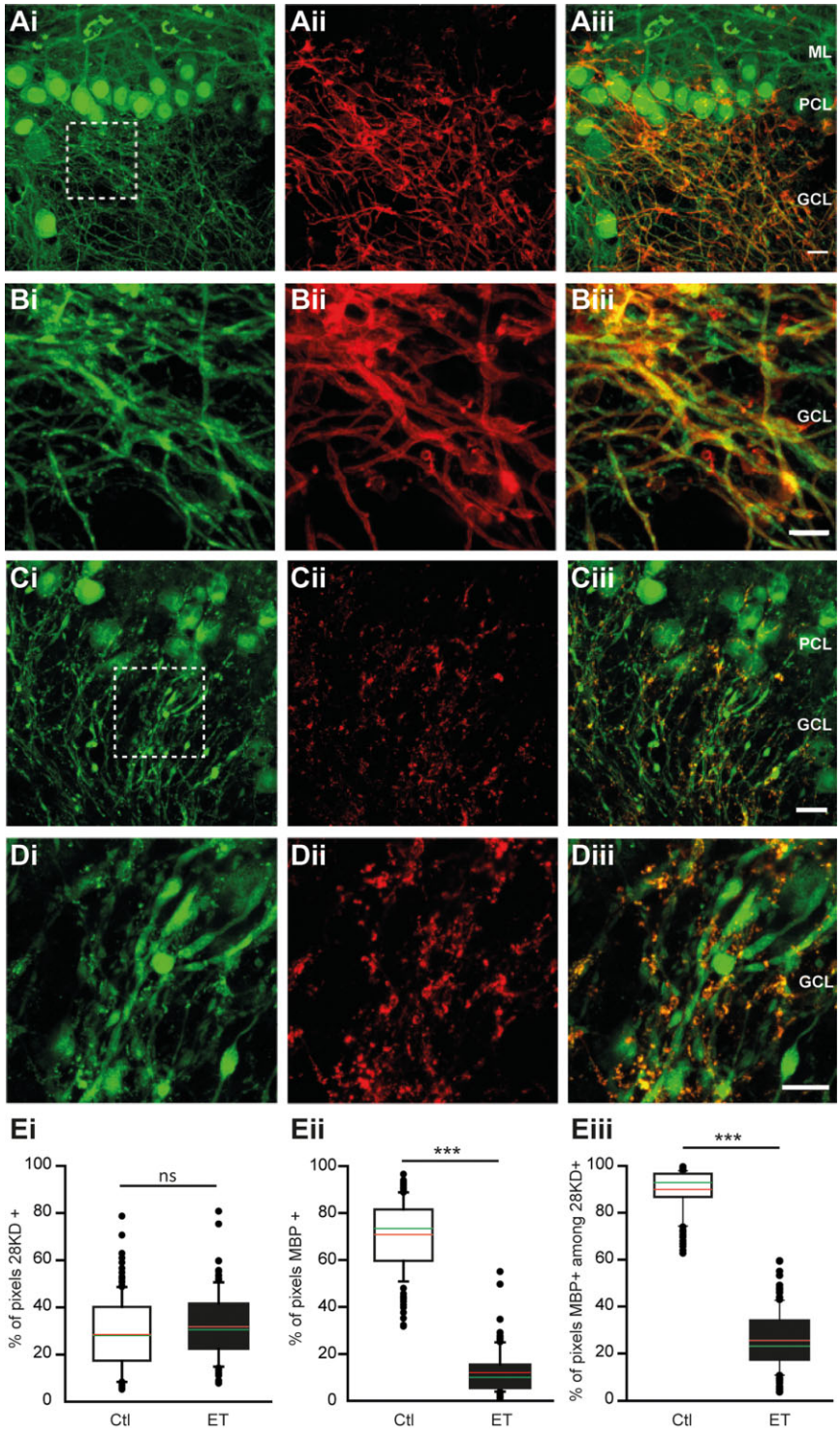


Fig. 7. ET-induced demyelination of Purkinje cell axons in organotypic culture of cerebellar slices. GCL, granule cells layer; PCL, Purkinje cells layer; ML, molecular layer.
A and C. Immunostaining of (i) the 28 kD protein (green, to label Purkinje cells), and (ii) MBP (red, to label myelin) in cerebellar slices maintained in organotypic cultures, treated without (A) or with (C) ET 10^{-7} M for 24 h. iii, their merged image. Scale bar = 25 μm.
B and D. Same presentation, except that magnifications of the regions denoted by a dotted frame in A and C are shown. Scale bar = 12.5 μm.
E. Quantification of the immunostaining of 28 kD and MBP determined from analysing ROI of 100 × 100 pixels selected in the granular layer. White-filled box plots are for slices that were not treated with ET ($n = 92$ ROI); black-filled box plots are for the ET-treated slices ($n = 116$ ROI). Horizontal lines denote medians (in red), and the means (in green). Ei. % of 28 kD+ pixels in ROI. Eii. % of MBP+ pixels in ROI. Eiii. % of 28 kD+ and MBP+ pixels. ***$P < 0.001$.

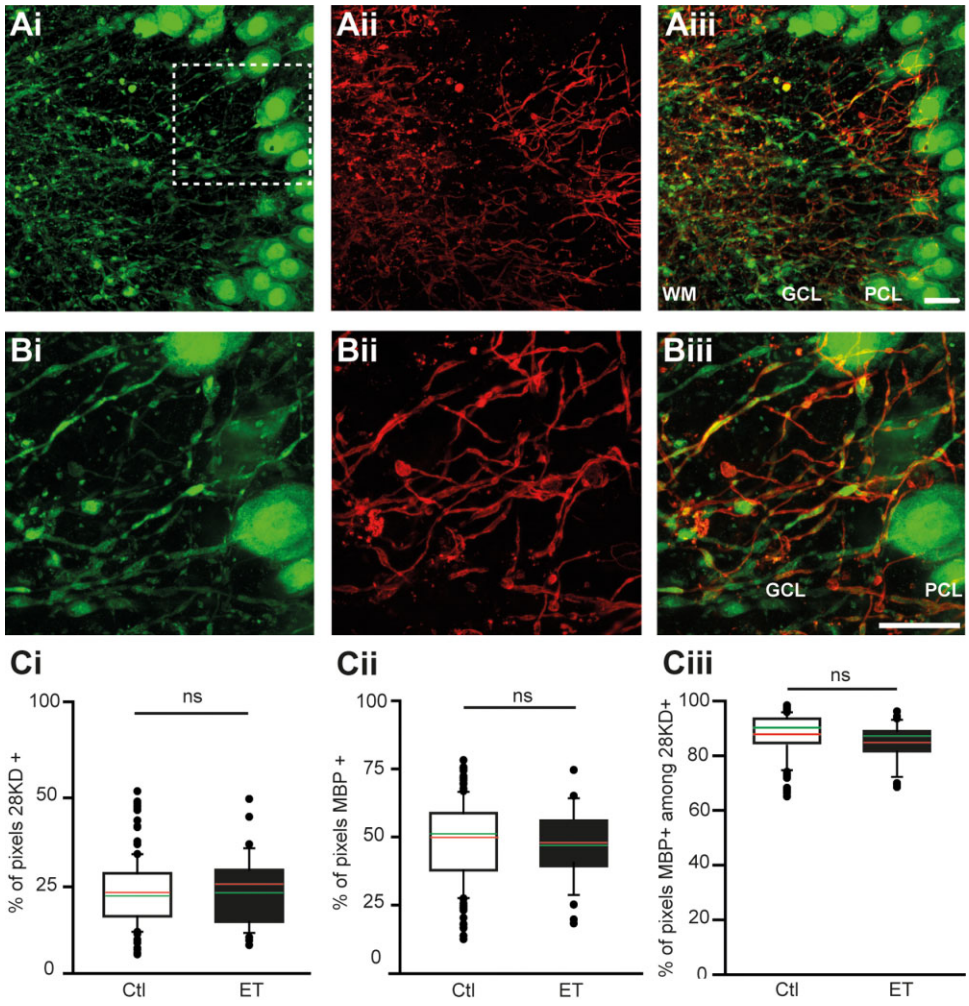


Fig. 8. Blocking mGluR1 and NMDA-R prevents ET-induced demyelination.
A, B. Same presentation as in Fig. 7C,D, except that ET 10^{-7} M was applied to the cerebellar slices in organotypic culture for 24 h in a culture medium containing specific antagonists of the NMDA-R (D-APV, 5 10^{-5} M) and mGluR1 ($JNJ_{16259685}$, 2 10^{-6} M).
C. The corresponding quantifications (same presentation as in Fig. 7E), after treating the slices without (white box plots, $n = 100$ ROI) or with (black box plots, $n = 100$ ROI) ET 10^{-7} M with D-APV and $JNJ_{16259685}$ for 24 h.

Dorca-Arévalo *et al.*, 2008; Lonchamp *et al.*, 2010). As ET-induced $[glutamate]_e$ increase (the primary action of ET on oligodendrocytes, as discussed later) can be neutralized by specific anti-ET antibodies, the various manifestations we describe here (i.e. initial rise in $[glutamate]_e$ and ensuing $[Ca^{2+}]_i$ oscillations and demyelination) are therefore the consequences of the specific binding of ET to the oligodendrocytes (Fig. 9, step 1). As this toxin binding and the consequent manifestations are detected using 10^{-9} M ET, oligodendrocytes probably express high-affinity ET receptor(s). In primary cultures, some oligodendrocytes are not targeted by ET (~ 20% using 10^{-7}M ET), while some others do not respond to ET by initiating intracellular Ca^{2+} events. Thus, ET-receptor is expressed in a subset (~ 80%) of oligodendrocytes and all the observed ET effects are primarily induced by ET action on these cells.

ET does not form pores in oligodendrocytes

ET forms pores that are characterized by a very high conductance (~ 500 pS) (Petit *et al.*, 2001; Nestorovich *et al.*, 2010). Therefore, the presence of just one pore can cause a marked decrease in R_m. The pore-forming activity of ET is confirmed in certain cell types, as denoted by a marked ET-induced decrease in R_m within renal collecting duct mpkCCDcl4 cells and neurons (Chassin *et al.*, 2007; Lonchamp *et al.*, 2010). It is crucial to note that while ET induces several cell effects (i.e. $[glutamate]_e$ rise and intracellular $[Ca^{2+}]$-oscillations) at low concentrations (10^{-9} M), high concentrations (10^{-7} M) do not induce any decrease in R_m, even under conditions permitting the detection of a single ET pore (for more details, see Ba^{2+} experiments). ET therefore acts on oligodendrocytes without forming pores. This is supported by evidence that

© 2014 The Authors. Cellular Microbiology published by John Wiley & Sons Ltd,

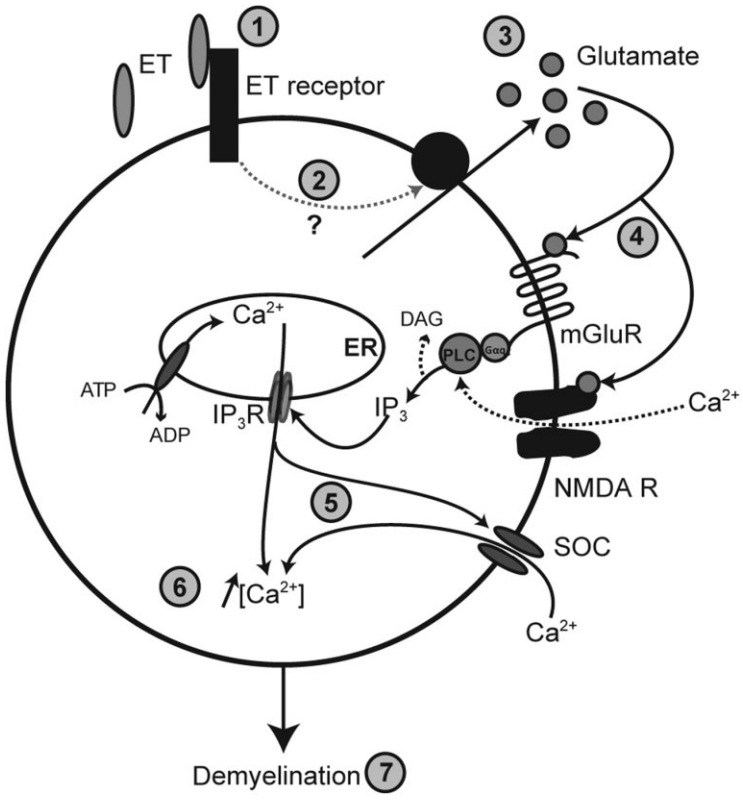


Fig. 9. Schematic representation of the cascade of ET effects in oligodendrocytes. Following its binding to high-affinity receptor(s) (step 1), ET activates an as yet unidentified pathway, causing alteration in membrane glutamate transport (step 2). The resulting increase in $[glutamate]_e$ (step 3) induces autocrine activation of mGluR-1 (step 4), possibly benefiting from synergistic activation of NMDA-R. This is followed (step 5) by production of IP_3, the activation of IP_3-R, Ca^{2+} release from ER and possibly store-operated channel (SOC)-mediated Ca^{2+}-entry, causing $[Ca^{2+}]_i$ oscillations (step 6). This triggers demyelination (step 7).

despite the capacity of ET pores to accommodate a transmembrane flux of soluble small molecules of up to ~ 2300 Da from the intracellular side (Nestorovich *et al*., 2010), there is no leakage of the Ca^{2+}-fluorescent probe Oregon Green BAPTA-1 (MW ~ 500 Da), the basal fluorescence of which remains stable over the whole duration of the experiments (Figs 5 and 6). Our study is the first to provide compelling evidence that ET can act on target cells without creating pores, and shows that ET binding to specific receptors (Fig. 9, step 1) activates pathway(s) that mediate the manifestations induced by the toxin.

An increase in $[glutamate]_e$ results from direct primary action of ET on oligodendrocytes

The collective evidence provided in this paper fully supports the possibility that a direct action of ET on oligodendrocytes causes rapid $[glutamate]_e$ elevation (Fig. 9, step 3). This raises the question of the possible mechanisms involved. Although glutamate is small enough (~ 150 Da) to pass through ET pore lumen and certain other types of membrane channels (Nedergaard *et al*., 2002), the lack of any ET-induced change in R_m rules out this possibility. Glutamate leakage because of oligodendrocyte plasma membrane severing is also unlikely. Indeed, despite the fact that about 80% of these cells respond to ET (see the $[Ca^{2+}]_i$ oscillations), none of them die (no staining of oligodendrocytes by trypan blue up to 24 h after 10^{-7} M ET application) or show any evidence of plasma membrane rupture (the cytosolic enzyme glucose-6-phosphate hydrogenase is not detected in the extracellular compartment). It is also unlikely that the increase in ET-induced $[glutamate]_e$ results from glutamate exocytosis, a minor process in glial cells that is still under debate (Nedergaard *et al*., 2002; Hamilton and Attwell, 2010) and has not been described in oligodendrocytes to date. The most likely explanation is that ET acts on glutamate membrane transport (Fig. 9, step 2). Indeed, oligodendrocytes are key actors in the regulation of extracellular glutamate homeostasis (DeSilva *et al*., 2009). They express three excitatory amino acid transporters for glutamate (Domercq and Matute, 1999; Danbolt, 2001; Pitt *et al*., 2003; DeSilva *et al*., 2009), which are all blocked by TBOA (Shimamoto *et al*., 1998). In accordance with this notion, TBOA produced a high $[glutamate]_e$ increase in the primary cultures in the absence of ET. It is likely that the release and uptake of glutamate by both the oligodendrocytes and astrocytes in the primary culture are balanced in order to maintain a low basal level of extracellular glutamate. This means that an ET-induced alteration of this dynamic equilibrium may cause the observed increase in $[glutamate]_e$ by either increasing the release or inhibiting the uptake of glutamate. Our data do not permit us to discern between

these two opposite possibilities. Indeed, if ET favours the release of glutamate, the lack of further ET-induced glutamate increase after TBOA may result from glutamate depletion of TBOA-treated oligodendrocytes. Conversely, if ET inhibits glutamate uptake, such an effect cannot occur after prior inhibition of the transporter by TBOA. The primary cultures contained oligodendrocytes, but also a noticeable population of astrocytes. As these two cell types can release glutamate in response to a $[glutamate]_e$ increase (Nedergaard *et al*., 2002), it is possible that the $[glutamate]_e$ that we observed after ET treatment is the result of ET primary direct action on the oligodendrocytes, amplified by a glutamate-induced glutamate release by astrocytes. An important issue for future investigations is the deciphering of the signalling pathway linking ET binding to the changes in glutamate membrane transport (Fig. 9, step 2).

Intracellular [Ca^{2+}] oscillations and demyelination are indirect effects of ET, and result from the initial toxin-induced rise in $[glutamate]_e$

ET induces $[Ca^{2+}]_i$ oscillations in oligodendrocytes, which then cease upon the removal of extracellular Ca^{2+}, the blocking of the SERCA pump, or the addition of 2-APB (which blocks the IP_3-Rs and store-operated Ca^{2+} entry). However, these oscillations remain almost unaffected following the blockade of RyR. This is in line with current knowledge on Ca^{2+}-signalling in glial cells (Verkhratsky and Kettenmann, 1996; Butt, 2006; Nedergaard *et al*., 2010), and suggests that these ET-induced $[Ca^{2+}]_i$ oscillations may be primarily initiated by the release of Ca^{2+} into the cytosol from ER stores following the activation of the IP_3 pathway, and may implicate store-operated Ca^{2+} entry (Fig. 9, step 5). ET-induced Ca^{2+} signals in oligodendrocytes are prevented by specifically antagonizing mGluR1 with $JNJ_{16259685}$. Thus, the $[Ca^{2+}]_i$ oscillations (Fig. 9, step 6) are caused by activation of the mGluR1 (Fig. 9, step 4) in response to the $[glutamate]_e$ rise (Fig. 9, step 3) induced by the toxin. This accords with the view that glutamate induces calcium oscillations in glial cells (Charles *et al*., 1991; Cornell-Bell and Finkbeiner, 1991) and the mGluR – phospholipase C – IP_3-R pathway is a prominent one in oligodendrocytes (Luyt *et al*., 2003; 2006). The $[glutamate]_e$ measured after ET application is high enough (1–1.5 10^{-6} M, with higher values in the vicinity of the cells) to substantially activate mGluR1 (Conn and Pin, 1997), and also other types of glutamate receptors like the NMDA-R. Consistent with the earlier, we found that the activation of NMDA-R is synergistic with that of mGluR1 in order to induce $[Ca^{2+}]_i$ oscillations, as suggested by delayed Ca^{2+} events when NMDA-R is blocked by D-APV. The prominent ET-induced demyelination (Fig. 9, step 7) in cultured slices is also a secondary effect caused by the toxin-induced $[glutamate]_e$ increase. Indeed, ET-induced demyelination is prevented by mGluR1 and NMDA-R antagonists (Fig. 9, step 4).

Overall, these data are fully consistent with the notion that oligodendrocytes are highly vulnerable to glutamate-dependent excitotoxic insults (reviewed in Matute *et al*., 2006; Matute, 2011), and that a $[glutamate]_e$ increase causes myelin alterations (Smith *et al*., 2000; Matute *et al*., 2001; Kostic *et al*., 2013).

As demyelination is not a primary action of ET, but rather an indirect consequence of toxin-induced oligodendrocyte-dependent elevation of $[glutamate]_e$, it is possible that cells (neurons, astrocytes or microglia) that are not directly targeted by ET may contribute to the amplification of ET action on oligodendrocytes. For instance, glutamate-induced glutamate release by astrocytes (discussed earlier) may allow $[glutamate]_e$ to reach sufficiently high levels to activate Ca^{2+} signalling and demyelination. Such synergistic action between oligodendrocytes and astrocytes accords with the notion that glutamate release by astrocytes may cause demyelination (Matute *et al*., 2006; Matute, 2011).

An important point is that the demyelination process does not necessarily involve the death of the oligodendrocytes. Indeed, elevated $[Ca^{2+}]_i$ can trigger myelin alteration by remodelling the intracellular cytoskeleton (reviewed in Harauz and Boggs, 2013). Therefore, consistent with our observation that ET does not kill oligodendrocytes (see the trypan blue experiments), it is likely that the glutamate-induced $[Ca^{2+}]_i$ oscillations signal the demyelination process. Note also that the changes in $[Ca^{2+}]_i$ consist of repeated brief oscillations that prevent $[Ca^{2+}]_I$ from building up and probably keep levels below the threshold for apoptosis or necrosis.

Does ET cause demyelination in vivo*?*

Damage to white matter has been reported in cases of *C. perfringens* B or D enterotoxaemia in ruminants (Buxton and Morgan, 1976; Finnie, 1984a,b; Uzal and Kelly, 1997; Uzal *et al*., 1997). However, it remains unclear whether they are caused by oedemas or ET-induced demyelination. Indeed, no demyelination has been described in these studies. It is possible that the death caused by this disease occurs too quickly to induce any noticeable demyelination. Although humans are not usual targets for ET, a study published a short time ago reported the increased frequency of ET immunoreactivity in the sera and cerebrospinal fluid of patients suffering from multiple sclerosis (Rumah *et al*., 2013) – a white matter disease caused by demyelination.

To conclude, this study reveals that ET, a bacterial toxin previously reported as damaging its cell targets via the formation of pores, can act at low concentrations (10^{-9} M)

© 2014 The Authors. Cellular Microbiology published by John Wiley & Sons Ltd,

on certain cells without forming pores. In oligodendrocytes, the different cell manifestations are organized into a cascade of effects (summarized in Fig. 9) initiated by ET binding to its receptor. As ET induces demyelination *in vitro*, this toxin can be considered as a causal candidate, among others, in the initial events of certain myelin pathologies.

Experimental procedures

Ethics statement

All experimental procedures are in accordance with European and French guidelines for animal experimentation and have been approved by the Bas-Rhin veterinary office, Strasbourg, France (authorization number 67-26 to BP) and by the Paris veterinary office, France (authorization number 75–279 to MP).

Rat cerebellar slices

P20-P30 Wistar rats (Animal facility of CNRS-Strasbourg University, UMS3415 Chronobiotron) were decapitated after isoflurane general anaesthesia. Acute slices (150 μm thick) were prepared from rat cerebellum following the protocol described by Lonchamp *et al*. (2010), but using a Microm HM650V slicer (Thermo Scientific). Slices were maintained in ice-cold artificial cerebrospinal fluid (ACSF) bubbled with carbogen (95% O2 and 5% CO_2) (Lonchamp *et al*., 2010).

Cerebellar primary cultures containing oligodendrocytes and astrocytes

Primary cultures of newborn (P0–P1) Wistar rat cerebellum (Animal facility of CNRS-Strasbourg University, UMS3415 Chronobiotron) were prepared as detailed by Gaillard and Bossu (1995) and Boussouf *et al*. (1997). In essence, the culture conditions were designed in order to select cell types of interest while eliminating certain others. To allow the growth of glial progenitors while preventing the survival of neurons, freshly dissociated cerebellar cells were re-suspended in Dulbecco/Vogt modified Eagle's minimal essential medium (DMEM) supplemented with high glucose as described by Gaillard and Bossu (1995) and Boussouf *et al*. (1997) and containing 5% decomplemented horse serum and 5% decomplemented foetal calf serum. When cultured in this medium for 6 days (with a change of medium every 2 days), cells were comprised of progenitor glial cells and astrocytes, but no oligodendrocytes (Boussouf *et al*., 1997). To obtain cultures containing a maximum number of oligodendrocytes, but the lowest possible amount of astrocytes, the cells were rinsed after 2 days of culture in the aforementioned medium and exposed to a serum-free, chemically defined medium consisting of DMEM supplemented with high glucose, as previously described (Gaillard and Bossu, 1995; Boussouf *et al*., 1997). Experiments based on oligodendrocytes were performed at least 4 days after transfer to this second stage of culture. As some Petri dishes could contain some residual granule cells, the culture dishes were checked under the microscope prior to any experiment, and were eliminated if contaminated by more than 1.5% of granule cells.

Organotypic culture of cerebellar slices

P10–P11 Wistar rats were anaesthetized by inhalation of isoflurane before decapitation. According to established methods (Stoppini *et al*., 1991), cerebella were dissected out into cold (4°C) minimum essential medium (MEM, Fisher). Parasagittal slices (300 μm thick) were made using a McIlwain tissue chopper (Mickle) and separated gently in cold MEM. The slices were then transferred onto Milicell cell culture inserts (Millipore), placed in six-well plates, containing 1 ml of culture medium composed of 50% MEM, 25% basal medium eagle (Fisher), 25% heat-inactivated horse serum, and supplemented with 2 10^{-3} M GlutaMAX™ (Fisher), 50 UI ml^{-1} penicillin, 50 μg ml^{-1} streptomycin and 4 g l^{-1} glucose. The cultures were incubated at 37°C in a humidified incubator equilibrated with 95% air/5% CO_2. Slices were cultured for 6 days to allow the myelination of Purkinje cells. The medium was completely changed every 2 days.

ET materials and neutralization

ET was purified from an overnight culture of *C. perfringens* type D strain NCTC2062, as previously described (Petit *et al*., 1997). The purity of ET (> 90%) was checked using sodium dodecyl sulfate polyacrylamide gel electrophoresis. Aliquots of ET were stored at −80°C. Specific anti-ET antibodies were raised in rabbits by subcutaneous injections of formalin-treated wild-type ET then immunopurified using wild-type ET bound to CNBr-activated Sepharose 4B column (GE Health Care). The neutralizing activity of the anti-ET antibodies was assessed in Madin-Darby canine kidney (MDCK) cells. Serial dilutions of anti-ET antibodies were mixed with fixed concentrations of ET for 30 min at RT then applied to MDCK cell monolayers grown on 96-well plates. Cell viability was monitored using the 3-(4,5-dimethylthiazol-2-yl)-2,5-diphenyltetrazolium bromide tetrazolium reduction (MTT) assay, as described by Petit *et al*. (2001) 3 h after incubation at 37°C. Using 10^{-9} M ET, a complete neutralization was obtained with 10^{-9} M-specific anti-ET antibodies, whereas when 10^{-8} ET was used, a 10-fold increase in anti-ET antibodies (10^{-7} M) versus ET was required for a complete neutralization.

Extracellular working solutions

Overall, experiments on primary cultures were performed using an external working solution containing (in 10^{-3} M): 140 NaCl, 5.4 KCl, 0.4 KH_2PO_4, 1 $CaCl_2$, 1 $MgCl_2$, 0.8 $MgSO_4$, 5 D^+-galactose, 10 glucose and 20 4-(2-hydroxyethyl)-1-piperazineethanesulfonic acid (HEPES), adjusted at 7.4 with NaOH (Gaillard and Bossu, 1995). For electrophysiological recordings, the working medium was modified by a solution containing (in 10^{-3} M): 145 NaCl, 5.4 KCl, 2 $CaCl_2$, 2 $MgCl_2$, 10 HEPES/Tris, 10 glucose and 10 sucrose. The pH was adjusted to 7.4 with TrisOH. When needed, 10^{-4} M $BaCl_2$ was added to the working external medium prior to recordings. Experiments on acute and organotypic slices were performed using the ACSF as working medium. To avoid non-specific adsorption of ET, all of the mediums were supplemented with bovine serum albumin (BSA, 2%). ET and/or various pharmacological agents were diluted in this medium at the desired concentrations.

ET detection and the immunochemistry of specific markers

Cerebellar acute slices, organotypic slices and cerebellar primary cultures were pre-incubated with BSA (2%, in working solution) before being submitted to ET (at the concentration indicated, for 10 min, at RT). They were then fixed using paraformaldehyde 4% in phosphate buffer solution (PBS) at RT (30 min), followed by transfer to a cold (4°C) saturation solution containing PBS with 0.2% Triton (to allow permeabilization), 2% BSA and 10% normal goat serum (Millipore), overnight. To reveal ET bound to its target cells, the primary anti-toxin antibodies (see earlier) were applied overnight (dilution 1/500) at 4°C or 2 h at RT under agitation. Secondary anti-rabbit antibodies tagged with Alexa 488 (Molecular Probes) were applied overnight at 4°C or 2 h at RT under agitation. To identify the ET-targeted cells in slices or in cultures, a similar protocol to the one detailed earlier was used, except that immunolabelling of ET and the cell markers of interest were run simultaneously (overnight at 4°C, or 2 h at RT under agitation), followed by three washes in the saturation solution and an overnight application of secondary antibodies (or 2 h at RT under agitation). Specific antibodies against the following markers were used: MBP (anti-MBP, ABD Serotec, rat monoclonal, 1/500), GFAP (anti-GFAP, Sigma-Aldrich, mouse monoclonal diluted 1/400), Iba-1 (Wako, rabbit polyclonal, 1/300) and 28 kD protein (also known as Calbindin, Sigma-Aldrich, mouse monoclonal, 1/1500). Finally, fixed slices or cut out 35 mm dishes containing primary cultures were mounted on glass coverslips with Prolong® Gold antifade reagent (Molecular Probes). Confocal images were produced at the In vitro Imaging Facility of the Neuropôle/Centre de Neurochimie de Strasbourg (France), using a Leica SP5II inverted confocal microscope (10×; 20× or 63× objectives). Fields of 1024 × 1024 pixels were acquired using 405 nm diode (ultraviolet), 488 nm argon laser (green), and 561 nm Diode-pumped solid-state laser (red).

Electrophysiological determination of passive plasma membrane resistance in cultured oligodendrocytes

Whole-cell membrane recordings were made using 5 MΩ microelectrode and the patch-clamp technique, as detailed by Lonchamp *et al*. (2010). Oligodendrocytes were identified on the basis of their typical morphology (40× objective, differential interference contrast (DIC) mode). Only cells presenting a resting transmembrane potential below −40 mV were used. Transmembrane potential was held at −60 mV, then passive transmembrane resistance (R_m) was determined at RT from the current changes (ΔI) induced by a series of hyperpolarizing and depolarizing square pulses (ΔV, 200 ms duration, increasing by 4 mV steps), under voltage-clamp. This protocol was repeated once a minute for the whole duration of the experiment. For each set of data (i.e. a protocol), R_m was determined by averaging the $\Delta V/\Delta I$ values, or from linear fitting of $\Delta I = f(\Delta V)$ plots.

Glutamate assay

Determination of extracellular concentration of glutamate was determined as described in Lonchamp *et al*., 2010; Jover *et al*., 2013 using the Amplex™ Red Glutamic Acid/Glutamate Oxidase Assay Kit (Molecular Probes), except that cells were cultured on 35 mm culture dishes. The calibration for each experiment was performed from a standard curve established using samples of the working solution containing known concentrations of glutamate. The determination of the maximal possible external concentration of glutamate was determined by lysing the cells with a hypo-osmotic shock (distilled water containing 10^{-2} M Tris-HCl, pH 7.4). The basal concentration (i.e. control) was measured by incubating the cells with the working medium without ET.

Glucose-6-phosphate dehydrogenase (G6PDH) assay

The extracellular activity of G6PDH was measured as described (Batchelor and Zhou, 2004; Jover *et al*., 2013). In essence, the experimental protocol was similar to that used for the glutamate assay except for the 50 µl reagent, which contained 2 10^{-3} M glucose-6-phosphate, 1.5 10^{-5} M resazurin, 0.5 10^{-3} M nicotinamide adenine dinucleotide phosphate (NADP) and 0.5 U ml^{-1} diaphorase. Activity of the G6PDH after ET application or cell lysis was normalized to that determined under control condition.

Test of cell viability

A trypan blue exclusion test of cell viability was carried out in order to detect oligodendrocyte death or survival after the exposure of cultures to ET (10^{-7} M) for 1, 3 or 24 h. Cell death was confirmed by the uptake of trypan blue following the incubation of the cultures with the dye [0.2 ml of a 0.4% trypan blue stock solution (Gibco) was added to 1 ml of the extracellular medium] for 10 min.

Calcium imaging

Intracellular calcium changes were monitored using the cell permeable AM ester form of the calcium fluorescent indicator Oregon Green BAPTA-1. Cerebellar primary cultures were incubated for 30 min at 37°C with Oregon Green BAPTA-1 and pluronic acid (4 10^{-6} M each, Invitrogen), then washed for 30 min at 37°C in the working solution, with or without drugs depending on the experimental conditions used. An upright microscope (Olympus BX51WI) was used to identify oligodendrocytes on the basis of their typical morphology using a plan NEOFLUAR ×40 0.80 objective (Zeiss) in the DIC mode. Single-cell measurements of $[Ca^{2+}]_i$ changes were then performed by exciting intracellular Oregon Green BAPTA-1 at 494 nm with a light-emitting diode (Thorlabs) and recording the emitted fluorescence image at 590 nm using a CoolSNAP HQ^2 camera (Photometrics), one frame every 0.5 s throughout the experiments. We analysed fluorescence in an ROI that covered the cell body of an oligodendrocyte in a culture dish without overlapping neighbouring cells. Dye excitation, image acquisitions and ROI analysis protocols were performed using WinFluor image analysis software (Strathclyde University). Relative changes in fluorescence intensity were expressed as the ratio $\Delta F/F$. $\Delta F/F = (F - F_0)/(F_0 - B)$, where F is the measured fluorescence intensity of Oregon Green, F_0 the fluorescence intensity of the indicator in the cell before stimulation (ET application), and B the background signal determined in a ROI adjacent to the cell.

Quantification of Purkinje cell myelination in cultured slices

Myelination of the Purkinje cells in cerebellar organotypic slices submitted to various treatments (ET and/or other drugs) was evaluated on fixed (4% paraformaldehyde) slices by revealing immunoreactivity against 28 kD protein (calbindin, to reveal Purkinje cells and their processes as axons) and MBP (to mark myelin). Confocal images (1024 × 1024, magnification of 20×, pixel size = 757 nm) were acquired using 500–530 nm (green) and 560–615 nm (red) filters. Non-overlapping ROI (100 × 100 pixels) were selected in the granule cell layer, just below the Purkinje cell layer. As the myelin sheet wraps around axons, 28 kD protein and MBP signals cannot co-localize well. Therefore, for each ROI and for each channel, the threshold of signal intensity was adjusted to 10% of the maximum pixel intensity, then the number of positive pixels for MBP (MBP+ pixels) and/or 28 kD protein (28 kD+ pixels) were counted.

Other materials

The following drugs were used at the indicated final concentration: Thapsigargin (0.5 10^{-6} M, Sigma-Aldrich), Dantrolene (1 10^{-5} M, Tocris), 2-APB (2-aminoethoxydiphenyl borate, 10^{-4} M, Tocris), $JNJ_{16259685}$ (2 10^{-6} M, Tocris), TBOA (threo-beta-benzyloxyaspartate, 10^{-4} M and Tocris). All these drugs were prepared as stock solutions diluted in dimethyl sulphoxide (DMSO) in such a way that the final concentration of DMSO in working solutions was < 0.1%. D-APV [(2*R*)-amino-5-phosphonovaleric acid, 5 10^{-5} M, Ascent] and glutamate (10^{-5} or 10^{-6} M, Sigma-Aldrich) were dissolved extemporaneously in distilled water before dilution to the desired final concentrations in the extracellular medium. Amphotericin B (AmB) and caffeine were from Sigma.

Statistical analysis

Where necessary, results are presented as mean ± SE established from the indicated number *n* of experiments. When data are not normally distributed, their median is also reported. We tested the statistical significance of the differences between two conditions, using Student *t*-tests (normally distributed data) or the Mann–Whitney test (not normally distributed data) for unpaired set of data, and the paired *t*-test for paired data. For comparisons of more than two conditions, statistical significance was tested using analysis of variance (normally distributed data) or the Kruskal–Wallis rank test (non-normally distributed data). *P* value > 0.05 denotes no significant difference (n.s.). Significant *P* is mentioned.

Acknowledgements

We thank the In Vitro Imaging Facility of the Neuropôle/Centre de Neurochimie de Strasbourg (France), Sophie Reibel and the animal facility Chronobiotron (UMS3415 CNRS and Strasbourg University). We are also grateful to Dorine Neel for her technical contribution to the initial demyelination experiments. The experimental work was supported by a doctoral grant from the Mission pour la Recherche et l'Innovation Scientifique – Délégation Générale à l'Armement (MRIS/DGA) for L.W., and by CNRS funding for B.P. The funders had no role in study design, data collection and analysis, decision to publish, or preparation of the paper. None of the results obtained are part of a patent or commercial product. J-L.D., F.D., S.G., P.I., J-L.B. and B.P. are permanent staff of the CNRS, F.H. is a non-permanent CNRS staff member, and S.P. and M.R.P. are permanent staff of the Institut Pasteur, Paris. The above does not alter the authors' adherence to all OnlineOpen policies on sharing data and materials.

References

Alberdi, E., Sánchez-Gómez, M.V., and Matute, C. (2005) Calcium and glial cell death. *Cell Calcium* **38:** 417–425.

Bakiri, Y., Burzomato, V., Frugier, G., Hamilton, N.B., Káradóttir, R., and Attwell, D. (2009) Glutamatergic signaling in the brain's white matter. *Neuroscience* **158:** 266–274.

Batchelor, R.H., and Zhou, M. (2004) Use of cellular glucose-6-phosphate dehydrogenase for cell quantitation: applications in cytotoxicity and apoptosis assays. *Anal Biochem* **329:** 35–42.

Bernard, F., Bossu, J.L., and Gaillard, S. (2001) Identification of living oligodendrocyte developmental stages by fractal analysis of cell morphology. *J Neurosci Res* **65:** 439–445.

Bokori-Brown, M., Savva, C.G., Fernandes da Costa, S.P., Naylor, C.E., Basak, A.K., and Titball, R.W. (2011) Molecular basis of toxicity of *Clostridium perfringens* epsilon toxin. *FEBS J* **278:** 4589–4601.

Boussouf, A., Lambert, R., and Gaillard, S. (1997) Voltage dependant Na+ /HCO3-Cotransporter and Na+/H + exchanger are involved in intracellular pH regulation of cultured mature rat cerebellar oligodendrocytes. *Glia* **19:** 74–84.

Butt, A.M. (2006) Neurotransmitter-mediated calcium signalling in oligodendrocyte physiology and pathology. *Glia* **54:** 666–675.

Buxton, D., and Morgan, K.T. (1976) Studies of lesions produced in the brains of colostrum deprived lambs by *Clostridium welchii* (*Cl. perfringens*) type D toxin. *J Comp Pathol* **86:** 435–447.

Charles, A.C., Merrill, J.E., Dirksen, E.R., and Sanderson, M.J. (1991) Intercellular signaling in glial cells: calcium waves and oscillations in response to mechanical stimulation and glutamate. *Neuron* **6:** 983–992.

Chassin, C., Bens, M., Barry, J., de Courjaret, R., Bossu, J.L., Cluzeaud, F., *et al.* (2007) Pore-forming epsilon toxin causes membrane permeabilization and rapid ATP depletion-mediated cell death in renal collecting duct cells. *Am J Physiol* **293:** 927–937.

Cohen, B.E. (2010) Amphotericin B membrane action: role for two types of ion channels in eliciting cell survival and lethal effects. *J Membr Biol* **238:** 1–20.

Cole, A.R., Gibert, M., Popoff, M., Moss, D.S., Titball, R.W., and Basak, A.K. (2004) *Clostridium perfringens* epsilon-toxin shows structural similarity to the pore-forming toxin aerolysin. *Nat Struct Mol Biol* **11:** 797–798.

Conn, P.J., and Pin, J.P. (1997) Pharmacology and functions of metabotropic glutamate receptors. *Annu Rev Pharmacol Toxicol* **37:** 205–237.

Cornell-Bell, A.H., and Finkbeiner, S.M. (1991) Ca2+ waves in astrocytes. *Cell Calcium* **12:** 185–204.

Danbolt, N.C. (2001) Glutamate uptake. *Prog Neurobiol* **65:** 1–105.

De Biase, L.M., Nishiyama, A., and Bergles, D.E. (2010) Excitability and synaptic communication within the oligodendrocyte lineage. *J Neurosci* **30:** 3600–3611.

DeSilva, T.M., Kabakov, A.Y., Goldhoff, P.E., Volpe, J.J., and Rosenberg, P.A. (2009) Regulation of glutamate transport in developing rat oligodendrocytes. *J Neurosci* **29:** 7898–7908.

Domercq, M., and Matute, C. (1999) Expression of glutamate transporters in the adult bovine corpus callosum. *Brain Res Mol Brain Res* **67:** 296–302.

Dorca-Arévalo, J., Soler-Jover, A., Gibert, M., Popoff, M.R., Martín-Satué, M., and Blasi, J. (2008) Binding of epsilon-toxin from *Clostridium perfringens* in the nervous system. *Vet Microbiol* **131:** 14–25.

Finnie, J. (2004) Neurological disorders produced by *Clostridium perfringens* type D epsilon toxin. *Anaerobe* **10:** 145–150.

Finnie, J.W. (1984a) Ultrastructural changes in the brain of mice given *Clostridium perfringens* type D epsilon toxin. *J Comp Pathol* **94:** 445–452.

Finnie, J.W. (1984b) Histopathological changes in the brain of mice given *Clostridium perfringens* type D epsilon toxin. *J Comp Pathol* **94:** 363–370.

Fusco, F.R., Martorana, A., Giampà, C., De March, Z., Vacca, F., Tozzi, A., *et al*. (2004) Cellular localization of TRPC3 channel in rat brain: preferential distribution to oligodendrocytes. *Neurosci Lett* **365:** 137–142.

Gaillard, S., and Bossu, J.-L. (1995) Voltage-gated ionic currents in mature oligodendrocytes isolated from rat cerebellum. *Neurosci Lett* **190:** 191–194.

Gill, D.M. (1982) Bacterial toxins: a table of lethal amounts. *Microbiol Rev* **46:** 86–94.

Gipson, K., and Bordey, A. (2002) Analysis of the K+ current profile of mature rat oligodendrocytes in situ. *J Membr Biol* **189:** 201–212.

Hagiwara, S., Miyazaki, S., Moody, W., and Patlak, J. (1978) Blocking effects of barium and hydrogen ions on the potassium current during anomalous rectification in the starfish egg. *J Physiol* **279:** 167–185.

Hamilton, N.B., and Attwell, D. (2010) Do astrocytes really exocytose neurotransmitters? *Nat Rev Neurosci* **11:** 227–238.

Harauz, G., and Boggs, J.M. (2013) Myelin management by the 18.5-kDa and 21.5-kDa classic myelin basic protein isoforms. *J Neurochem* **125:** 334–361.

Harteneck, C., and Gollasch, M. (2011) Pharmacological modulation of diacylglycerol-sensitive TRPC3/6/7 channels. *Curr Pharm Biotechnol* **12:** 35–41.

Hibino, H., Inanobe, A., Furutani, K., Murakami, S., Findlay, I., and Kurachi, Y. (2010) Inwardly rectifying potassium channels: their structure, function, and physiological roles. *Physiol Rev* **90:** 291–366.

Jover, E., Tawk, M.Y., Laventie, B.-J., Poulain, B., and Prévost, G. (2013) Staphylococcal leukotoxins trigger free intracellular Ca(2+) rise in neurones, signalling through acidic stores and activation of store-operated channels. *Cell Microbiol* **15:** 742–758.

Kostic, M., Zivkovic, N., and Stojanovic, I. (2013) Multiple sclerosis and glutamate excitotoxicity. *Rev Neurosci* **24:** 71–88.

Lavreysen, H., Wouters, R., Bischoff, F., Nóbrega Pereira, S., Langlois, X., Blokland, S., *et al*. (2004) $JNJ_{16259685}$, a highly potent, selective and systemically active mGlu1 receptor antagonist. *Neuropharmacology* **47:** 961–972.

Lonchamp, E., Dupont, J.-L., Wioland, L., Courjaret, R., Mbebi-Liegeois, C., Jover, E., *et al*. (2010) *Clostridium perfringens* epsilon toxin targets granule cells in the mouse cerebellum and stimulates glutamate release. *PLoS ONE* **5:** e13046.

Luyt, K., Varadi, A., and Molnar, E. (2003) Functional metabotropic glutamate receptors are expressed in oligodendrocyte progenitor cells. *J Neurochem* **84:** 1452–1464.

Luyt, K., Váradi, A., Durant, C.F., and Molnár, E. (2006) Oligodendroglial metabotropic glutamate receptors are developmentally regulated and involved in the prevention of apoptosis. *J Neurochem* **99:** 641–656.

McClane, B., Uzal, F., Fernandez-Miyakawa, M.E., Lyverly, D., and Wilkins, T. (2006) The enterotoxic clostridia. *Prokaryotes* **4:** 698–752.

Matute, C. (2011) Glutamate and ATP signalling in white matter pathology. *J Anat* **219:** 53–64.

Matute, C., Alberdi, E., Domercq, M., Pérez-Cerdá, F., Pérez-Samartín, A., and Sánchez-Gómez, M.V. (2001) The link between excitotoxic oligodendroglial death and demyelinating diseases. *Trends Neurosci* **24:** 224–230.

Matute, C., Domercq, M., and Sánchez-Gómez, M.-V. (2006) Glutamate-mediated glial injury: mechanisms and clinical importance. *Glia* **53:** 212–224.

Miyamoto, O., Minami, J., Toyoshima, T., Nakamura, T., Masada, T., Nagao, S., *et al*. (1998) Neurotoxicity of *Clostridium perfringens* epsilon-toxin for the rat hippocampus via the glutamatergic system. *Infect Immun* **66:** 2501–2508.

Miyamoto, O., Sumitani, K., Nakamura, T., Yamagami, S., Miyata, S., Itano, T., *et al*. (2000) *Clostridium perfringens* epsilon toxin causes excessive release of glutamate in the mouse hippocampus. *FEMS Microbiol Lett* **189:** 109–113.

Nagahama, M., and Sakurai, J. (1991) Distribution of labeled *Clostridium perfringens* epsilon toxin in mice. *Toxicon* **29:** 211–217.

Nedergaard, M., Takano, T., and Hansen, A.J. (2002) Beyond the role of glutamate as a neurotransmitter. *Nat Rev* **3:** 748–755.

Nedergaard, M., Rodríguez, J.J., and Verkhratsky, A. (2010) Glial calcium and diseases of the nervous system. *Cell Calcium* **47:** 140–149.

Nestorovich, E.M., Karginov, V.A., and Bezrukov, S.M. (2010) Polymer partitioning and ion selectivity suggest asymmetrical shape for the membrane pore formed by epsilon toxin. *Biophysj* **99:** 782–789.

Olsen, M., and Sontheimer, H. (2008) Functional implications for Kir4.1 channels in glial biology: from K+ buffering to cell differentiation. *J Neurochem* **107:** 589–601.

Palay, S., and Chan-Palay, V. (1974) *Cerebellar Cortex: Cytology and Organization*. Berlin: Springer-Verlag.

Petit, L., Gibert, M., Gillet, D., Laurent-Winter, C., Boquet, P., and Popoff, M.R. (1997) *Clostridium perfringens* epsilon-

toxin acts on MDCK cells by forming a large membrane complex. *J Bacteriol* **179:** 6480–6487.

Petit, L., Maier, E., Gibert, M., Popoff, M.R., and Benz, R. (2001) *Clostridium perfringens* epsilon toxin induces a rapid change of cell membrane permeability to ions and forms channels in artificial lipid bilayers. *J Biol Chem* **276:** 15736–15740.

Petit, L., Gibert, M., Gourch, A., Bens, M., Vandewalle, A., and Popoff, M. (2003) *Clostridium perfringens* epsilon toxin rapidly decreases membrane barrier permeability of polarized MDCK cells. *Cell Microbiol* **5:** 155–164.

Pitt, D., Nagelmeier, I.E., Wilson, H.C., and Raine, C.S. (2003) Glutamate uptake by oligodendrocytes: implications for excitotoxicity in multiple sclerosis. *Neurology* **61:** 1113–1120.

Popoff, M.R. (2011) Epsilon toxin: a fascinating pore-forming toxin. *FEBS J* **278:** 4602–4615.

Robertson, S.L., Li, J., Uzal, F.A., and McClane, B.A. (2011) Evidence for a prepore stage in the action of *Clostridium perfringens* epsilon toxin. *PLoS ONE* **6:** e22053.

Rumah, K.R., Linden, J., Fischetti, V.A., and Vartanian, T. (2013) Isolation of *Clostridium perfringens* type B in an individual at first clinical presentation of multiple sclerosis provides clues for environmental triggers of the disease. *PLoS ONE* **8:** e76359.

Shimamoto, K., Lebrun, B., Yasuda-Kamatani, Y., Sakaitani, M., Shigeri, Y., Yumoto, N., and Nakajima, T. (1998) DL-threo-beta-benzyloxyaspartate, a potent blocker of excitatory amino acid transporters. *Mol Pharmacol* **53:** 195–201.

Smith, T., Groom, A., Zhu, B., and Turski, L. (2000) Autoimmune encephalomyelitis ameliorated by AMPA antagonists. *Nat Med* **6:** 62–66.

Soler-Jover, A., Dorca, J., Popoff, M.R., Gibert, M., Saura, J., Tusell, J.M., *et al*. (2007) Distribution of *Clostridium perfringens* epsilon toxin in the brains of acutely intoxicated mice and its effect upon glial cells. *Toxicon* **50:** 530–540.

Stoppini, L., Buchs, P.A., and Muller, D. (1991) A simple method for organotypic cultures of nervous tissue. *J Neurosci Methods* **37:** 173–182.

Takasaki, C., Yamasaki, M., Uchigashima, M., Konno, K., Yanagawa, Y., and Watanabe, M. (2010) Cytochemical and cytological properties of perineuronal oligodendrocytes in the mouse cortex. *Eur J Neurosci* **32:** 1326–1336.

Uzal, F.A., and Kelly, W.R. (1997) Effects of the intravenous administration of *Clostridium perfringens* type D epsilon toxin on young goats and lambs. *J Comp Pathol* **116:** 63–71.

Uzal, F.A., and Songer, J. (2008) Diagnosis of *Clostridium perfringens* intestinal infections in sheep and goats. *J Vet Diagnostic Investig* **20:** 253–265.

Uzal, F.A., Glastonbury, J.R., Kelly, W.R., and Thomas, R. (1997) Caprine enterotoxaemia associated with cerebral microangiopathy. *Vet Rec* **141:** 224–226.

Verkhratsky, A., and Kettenmann, H. (1996) Calcium signalling in glial cells. *Trends Neurosci* **19:** 346–352.

Verkhratsky, A., and Parpura, V. (2014) Store-operated calcium entry in neuroglia. *Neurosci Bull* **30:** 125–133.

Wioland, L., Dupont, J., Bossu, J., Popoff, M.R., and Poulain, B. (2013) Attack of the nervous system by *Clostridium perfringens* epsilon toxin: from disease to mode of action on neural cells. *Toxicon* **75:** 122–135.

Zhu, C., Ghabriel, M.N., Blumbergs, P.C., Reilly, P.L., Manavis, J., Youssef, J., *et al*. (2001) *Clostridium perfringens* prototoxin-induced alteration of endothelial barrier antigen (EBA) immunoreactivity at the blood–brain barrier (BBB). *Exp Neurol* **169:** 72–82.